



Michigan Technological University  
*Create the Future* Digital Commons @ Michigan Tech

---

Dissertations, Master's Theses and Master's  
Reports - Open

Dissertations, Master's Theses and Master's  
Reports

---

2011

## Dynamic modeling of active regeneration in catalyzed and non-catalyzed diesel particulate filters

Aamod Pethe  
*Michigan Technological University*

Follow this and additional works at: <https://digitalcommons.mtu.edu/etds>



Part of the [Mechanical Engineering Commons](#)

Copyright 2011 Aamod Pethe

---

### Recommended Citation

Pethe, Aamod, "Dynamic modeling of active regeneration in catalyzed and non-catalyzed diesel particulate filters", Master's Thesis, Michigan Technological University, 2011.  
<https://doi.org/10.37099/mtu.dc.etds/398>

Follow this and additional works at: <https://digitalcommons.mtu.edu/etds>



Part of the [Mechanical Engineering Commons](#)

DYNAMIC MODELING OF ACTIVE REGENERATION IN CATALYZED AND  
NON-CATALYZED DIESEL PARTICULATE FILTERS

By

Aamod Pethe

A THESIS

Submitted in partial fulfillment of the requirements for the degree of

MASTER OF SCIENCE  
(Mechanical Engineering)

MICHIGAN TECHNOLOGICAL UNIVERSITY

2011

© Aamod Pethe 2011

This thesis, "Dynamic Modeling of Active Regeneration in Catalyzed and Non-Catalyzed Diesel Particulate Filters," is hereby approved in partial fulfillment of the requirements for the degree of MASTER OF SCIENCE in MECHANICAL ENGINEERING

DEPARTMENT: Mechanical Engineering-Engineering Mechanics

Thesis Advisor

\_\_\_\_\_  
Dr Gordon G. Parker

Department Chair

\_\_\_\_\_  
Dr William W. Predebon

Date

\_\_\_\_\_

# **TABLE OF CONTENTS**

<b>LIST OF FIGURES .....</b>	<b>v</b>
<b>LIST OF TABLES .....</b>	<b>viii</b>
<b>ACKNOWLEDGEMENTS .....</b>	<b>ix</b>
<b>LIST OF ABBREVIATIONS.....</b>	<b>x</b>
<b>ABSTRACT .....</b>	<b>xi</b>
<b>1. INTRODUCTION.....</b>	<b>1</b>
1.1 Objectives of Research .....	2
1.2 Outline of Thesis.....	2
<b>2. BACKGROUND AND LITERATURE REVIEW.....</b>	<b>3</b>
2.1 Diesel Particulate Filters .....	3
2.2 Regeneration in a Diesel Particulate Filter .....	5
2.3 Pre-oxidation during regeneration .....	6
2.4 DPF Modeling Studies .....	7
<b>3. ACTIVE REGENERATION MODEL DESCRIPTION .....</b>	<b>11</b>
3.1 ‘Two soot’ Hypothesis.....	11
3.1.1 Non-catalyzed DPF .....	12
3.1.2 Catalyzed DPF.....	13
3.2 DPF PM Oxidation Model Assumptions.....	13
3.3 DPF PM Oxidation Kinetic Model .....	14
3.3.1 Inputs to the model.....	14
3.3.2 Equations of the Model.....	14
<b>4. EXPERIMENTAL DATA ACQUISITION .....</b>	<b>18</b>
4.1 PM Loading Experiment .....	18
4.2 Active Regeneration Experiment .....	20
4.2.1 Protocol of the experiment .....	20
4.2.2 Layout of the reactor .....	21
<b>5. RESULTS AND DISCUSSION.....</b>	<b>24</b>
5.1 Experimental Data Analysis.....	24
5.1.1 Non-Catalyzed DPF Data Analysis .....	26

5.1.2	Catalyzed DPF Data Analysis.....	31
5.2	Parameter Optimization Process Description.....	38
5.2.1	Kinetic Parameters .....	38
5.3	Optimization Problem Setup .....	39
5.3.1	Cost Function.....	40
5.4	Optimization Results .....	42
5.4.1	Results for non-catalyzed DPF samples .....	42
5.4.1.1	Arrhenius Parameters .....	47
5.4.1.2	Impact of other parameters .....	48
5.4.2	Results for catalyzed DPF samples .....	49
5.4.2.1	Arrhenius Parameters .....	52
5.4.2.2	Impact of other parameters .....	53
<b>6.</b>	<b>CONCLUSION AND FUTURE WORK .....</b>	<b>56</b>
	<b>REFERENCES .....</b>	<b>56</b>
	<b>APPENDIX A.....</b>	<b>60</b>

## **LIST OF FIGURES**

<b>Fig 2.1:</b> Schematic representation of a DPF .....	4
<b>Fig 2.2:</b> Schematic diagram of a DPF channel .....	5
<b>Fig 3.1:</b> Schematic diagram of PM types on the wall of a non-catalyzed DPF .....	12
<b>Fig 3.2:</b> Schematic diagram of PM types on the wall of a catalyzed DPF ....	13
<b>Fig 4.1:</b> Photograph of one of the mini DPF cores and holder .....	19
<b>Fig 4.3:</b> Layout of the reactor .....	22
<b>Fig 5.1:</b> Actual rate of PM oxidation for 3 different non-catalyzed substrates .....	26
<b>Fig 5.2:</b> Normalized rate of PM oxidation for 3 different non-catalyzed substrates .....	27
<b>Fig 5.3:</b> Normalized mass retained for three different non-catalyzed substrates .....	28
<b>Fig 5.4:</b> Experimental Arrhenius Plot for three different non-catalyzed substrates .....	28
<b>Fig 5.5:</b> Calculation of $\beta_h$ from experimental data (high conversion: $\sim 75 - 100\%$ ) .....	30
<b>Fig 5.6:</b> Calculation of $\beta_h$ from experimental data (high conversion: $\sim 15 - 75\%$ ) .....	31
<b>Fig 5.7:</b> Rate of PM oxidation for catalyzed and non-catalyzed cordierite samples .....	32
<b>Fig 5.8:</b> Rate of PM oxidation for catalyzed and non-catalyzed aluminum titanate samples.....	33
<b>Fig 5.9:</b> Rate of PM oxidation for all catalyzed samples .....	34

<b>Fig 5.11:</b> Normalized mass retained for three different catalyzed substrates .....	35
<b>Fig 5.12:</b> Experimental Arrhenius Plot for two different catalyzed substrates .....	36
<b>Fig 5.13:</b> Calculation of $\beta_h$ from experimental data (high conversion: $\sim 75 - 100\%$ ) – catalyzed samples.....	37
<b>Fig 5.14:</b> Calculation of $\beta_h$ from experimental data (high conversion: $\sim 15 - 75\%$ ) – catalyzed samples .....	37
<b>Fig 5.15:</b> Schematic of optimization routine .....	42
<b>Fig 5.16:</b> Cordierite non catalyzed sample- experimental versus simulated mass retained.....	43
<b>Fig 5.17:</b> Cordierite non catalyzed sample- experimental versus simulated mass retained – Error bar .....	43
<b>Fig 5.18:</b> $\text{AlTi}_2\text{O}_5$ non catalyzed sample- experimental versus simulated mass retained .....	44
<b>Fig 5.19:</b> $\text{AlTi}_2\text{O}_5$ non catalyzed sample- experimental versus simulated mass retained – Error bar.....	45
<b>Fig 5.20:</b> SiC non catalyzed sample- experimental versus simulated mass retained .....	45
<b>Fig 5.21:</b> SiC non catalyzed sample- experimental versus simulated mass retained- Error bar .....	46
<b>Fig 5.22:</b> Arrhenius plot of simulated parameters of the three non-catalyzed samples .....	48
<b>Fig 5.23:</b> Cordierite catalyzed sample- experimental v simulated mass retained .....	50
<b>Fig 5.24:</b> Cordierite catalyzed sample- experimental v simulated mass retained –Error bar.....	50

<b>Fig 5.25:</b> AlTi <sub>2</sub> O <sub>5</sub> catalyzed sample- experimental v simulated mass retained .....	51
<b>Fig 5.26:</b> AlTi <sub>2</sub> O <sub>5</sub> catalyzed sample- experimental v simulated mass retained- Error bar .....	51
<b>Fig 5.27:</b> Arrhenius plot of simulated parameters of the three catalyzed samples .....	53
<b>Fig A.1 :</b> Flowchart of the code .....	61



## **LIST OF TABLES**

<b>Table 1.1</b>	US EPA regulations for on-road heavy duty diesel engines (1) ....	1
<b>Table 2.1</b>	List of reported activation energies .....	10
<b>Table 5.1</b>	Mass of PM loading .....	25
<b>Table 5.2</b>	List of parameters .....	40
<b>Table 5.3</b>	Kinetic Parameters from optimization (non catalyzed) .....	46
<b>Table 5.4</b>	Kinetic Parameters from optimization (catalyzed) .....	52
<b>Table 5.5</b>	Kinetic Parameters from optimization (Cordierite) .....	54
<b>Table 5.6</b>	Kinetic Parameters from optimization (Aluminum Titanate) .....	55

## **ACKNOWLEDGEMENTS**

I would like to thank my advisor Dr Gordon Parker for his support and motivation throughout this thesis. It was a great honor to work with such an accomplished professor. Throughout my time at Michigan Tech, he has been instrumental in shaping my thought process and analytical ability required for any research work. His insightful observations and comments on the work presented in this thesis were vital for its completion. Thank you Dr Parker. I would also thank Dr John Johnson for his support and guidance throughout my graduate research which helped tremendously in the work presented in this thesis.

I would like to thank Navistar Inc. for the financial support during this project. It was a great professional learning experience working with the Advanced Aftertreatment team at Navistar Inc. - Ed Derybowski, Dr Brad Adelman, Vadim Strots and Dr Shyam Santhanam. I would like to thank you all for the guidance, especially while helping me with the technical aspects of the work presented in this thesis (and for answering the countless questions that came up from time to time).

I would also like to thank Josh Pihl of Oak Ridge National Laboratory and Minyong Zhou of Exova Ltd. for providing the technical data and the description of the experimental facility used for this project.

I would like to thank Harsha Surenahalli and Kiran Premchand for sharing their knowledge with me and providing help during the writing of this thesis.

I would like to thank my family for their constant encouragement not just during this thesis but during the entire duration of my graduate study. I would also thank my friends who studied along with me at Michigan Tech for the many unforgettable moments during our time in Houghton and Chicago.

## **LIST OF ABBREVIATIONS**

PM	Particulate Matter
EPA	Environmental Protection Agency
DPF	Diesel Particulate Filter
DOC	Diesel Oxidation Catalyst
VOF	Volatile Organic Fraction
TPO	Temperature Programmed Oxidation
TPD	Temperature Programmed Desorption
LE	Low activation energy
HE	High activation energy
CT	Catalyzed
EGR	Exhaust Gas Recirculation

## **ABSTRACT**

Particulate matter (PM) emissions standards set by the US Environmental Protection Agency (EPA) have become increasingly stringent over the years. The EPA regulation for PM in heavy duty diesel engines has been reduced to 0.01 g/bhp-hr for the year 2010. Heavy duty diesel engines make use of an aftertreatment filtration device, the Diesel Particulate Filter (DPF). DPFs are highly efficient in filtering PM (known as soot) and are an integral part of 2010 heavy duty diesel aftertreatment system.

PM is accumulated in the DPF as the exhaust gas flows through it. This PM needs to be removed by oxidation periodically for the efficient functioning of the filter. This oxidation process is also known as regeneration. There are 2 types of regeneration processes, namely active regeneration (oxidation of PM by external means) and passive oxidation (oxidation of PM by internal means).

Active regeneration occurs typically in high temperature regions, about 500 - 600 °C, which is much higher than normal diesel exhaust temperatures. Thus, the exhaust temperature has to be raised with the help of external devices like a Diesel Oxidation Catalyst (DOC) or a fuel burner. The O<sub>2</sub> oxidizes PM producing CO<sub>2</sub> as oxidation product.

In passive oxidation, one way of regeneration is by the use of NO<sub>2</sub>. NO<sub>2</sub> oxidizes the PM producing NO and CO<sub>2</sub> as oxidation products. The passive oxidation process occurs at lower temperatures (200 - 400 °C) in comparison to the active regeneration temperatures.

Generally, DPF substrate walls are washcoated with catalyst material to speed up the rate of PM oxidation. The catalyst washcoat is observed to increase the rate of PM oxidation.

The goal of this research is to develop a simple mathematical model to simulate the PM depletion during the active regeneration process in a DPF (catalyzed and non-catalyzed). A simple, zero-dimensional kinetic model was developed in MATLAB.

Experimental data required for calibration was obtained by active regeneration experiments performed on PM loaded mini DPFs in an automated flow reactor. The DPFs were loaded with PM from the exhaust of a commercial heavy duty diesel engine.

The model was calibrated to the data obtained from active regeneration experiments. Numerical gradient based optimization techniques were used to estimate the kinetic parameters of the model.

# **1. INTRODUCTION**

Most on road heavy duty diesel engines emit soot or particulate matter (PM), nitrogen oxides (NO<sub>x</sub>), carbon monoxide (CO) and hydrocarbons which are harmful to human health. These exhaust gases are regulated in various countries by their respective governing bodies. The Environmental Protection Agency (EPA) is responsible for setting the regulations for the US engine manufacturers. The EPA regulations for these emissions have tightened over the years. The EPA PM regulations are listed in Table 1.1 (adapted from reference (1)). Only PM values are shown as they are the focus of the research. Similar regulatory trends exist both in the European Union and Japan.

**Table 1.1**

US EPA regulations for on-road heavy duty diesel engines (1)

<b>YEAR</b>	<b>PM (g/bhp-hr)</b>
1990	0.60
1991	0.25
1994	0.10
1998	0.10
2002	0.10
2007	0.01
2010	0.01

In order to comply with these stringent regulations, a highly efficient aftertreatment technology to remove PM from the exhaust, the Diesel Particulate Filter (DPF), has been developed. In a DPF, the PM is accumulated in the filter material. To prevent over accumulation and resulting detrimental back pressure, PM must be oxidized. This process of PM oxidation is also known as '*regeneration*'. There are two main types of PM regeneration. A continuous but slow removal of PM via oxidation with NO<sub>2</sub> is commonly called '*passive oxidation*' while an infrequent but rapid removal of PM via oxidation with O<sub>2</sub> is commonly called '*active regeneration*'. The nomenclature 'passive' and 'active' indicate whether the reaction occurs under standard exhaust conditions or if deliberate changes to engine or exhaust conditions are

invoked. Theoretical details of PM oxidation are given in references (1) through (4).

This research aims at modeling the process of active regeneration using a simple kinetic model developed in MATLAB. A parameter optimization code was wrapped around the model to estimate the kinetic parameters for the PM oxidation during active regeneration.

## **1.1 Objectives of Research**

The main objectives of this research are:

1. Development of a simple model to simulate PM oxidation by  $O_2$  in reactor DPFs. The amount of PM loading in the DPF samples used in this research was 7 g/l.
2. Calibration of the model using experimental data obtained using a reactor bench to study the PM oxidation. Three different substrate materials with and without catalyst coatings were used in this study.

## **1.2 Outline of Thesis**

The second chapter gives background information on DPF operation and active regeneration. Past research pertaining to PM oxidation and its modeling are reviewed. The third chapter explains the kinetic model development effort. This includes the assumptions, hypothesis, chemical reactions and the differential equations contained in the PM oxidation model. The fourth chapter gives a brief description of the experimental setup used to obtain the data for model calibration. The fifth chapter discusses the results of the simulation and the calibration carried out with the aid of numerical optimization techniques. The focus is on calibration differences resulting from different substrates and catalyst treatment. The sixth chapter consists of and suggestions for future work that could be proposed to further this research.

## **2. BACKGROUND AND LITERATURE REVIEW**

In order to understand the aspects related to active regeneration modeling in a DPF, a literature review was performed. Various publications were reviewed for this purpose. Peculiar patterns, especially pre-oxidation of PM during regeneration (explained in section 2.3), have been observed in the experimental data used in this research. Therefore studies which observed similar behavior were of particular interest.

### **2.1 Diesel Particulate Filters**

A Diesel Particulate Filter (DPF) is an aftertreatment device employed to reduce soot or particulate matter (PM) emissions produced from a diesel engine. The most common particulate filter design is the wall-flow monolith shown in the Figure 2.1. The DPF substrate wall is made from porous ceramic materials such as cordierite ( $2\text{MgO}_2\text{Al}_2\text{O}_3\cdot 5\text{SiO}_2$ ), aluminum titanate ( $\text{AlTi}_2\text{O}_5$ ), or silicon carbide (SiC). The opposite ends of alternate channels of the filter are plugged with an impermeable and thermally-stable material. This causes the exhaust gas which contains the soot or PM to enter the inlet channel and flow through the porous substrate wall of the filter to the outlet channel. The horizontal lines in the side view of Figure 2.1 represent the porous substrate wall of the filter. The shaded areas in both views represent the end plugs of the individual channels.

In a clean DPF filter, PM from the exhaust gets trapped in and on the filter walls. As exhaust gas flows through the DPF, PM accumulates on the filter forming what is called a 'PM cake layer'. This PM cake is also highly porous (about 99% filtration efficiency) and it filters the exhaust gas causing more PM deposition on the cake. This is called cake filtration and occurs after a threshold amount of cake layer thickness is formed. As the PM cake layer grows it causes the pressure drop across the DPF to increase. This causes degradation in fuel economy. Thus, there is a need to remove this PM layer during engine operation. Details of the DPF structure and filtration mechanisms are explained in references (1) through (4).

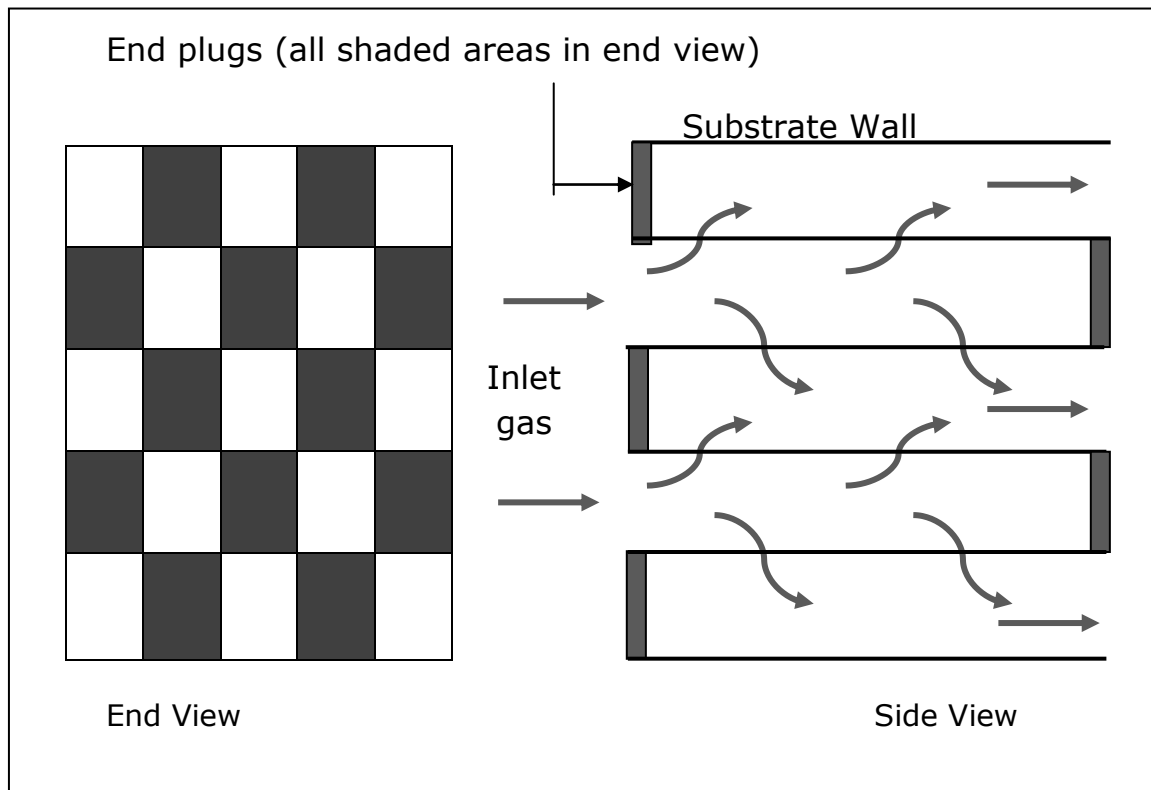


**Fig 2.1:** Schematic representation of a DPF, adapted from reference (1)

Figure 2.2 shows a single channel of DPF loaded with PM. If the surface of the substrate wall is washcoated with a catalyst, some of the PM particles will be in contact with the catalyst. Depending on the contact of PM particles with catalyst, reaction rates of oxidation will vary. This is explained in Neeft et al. (5).



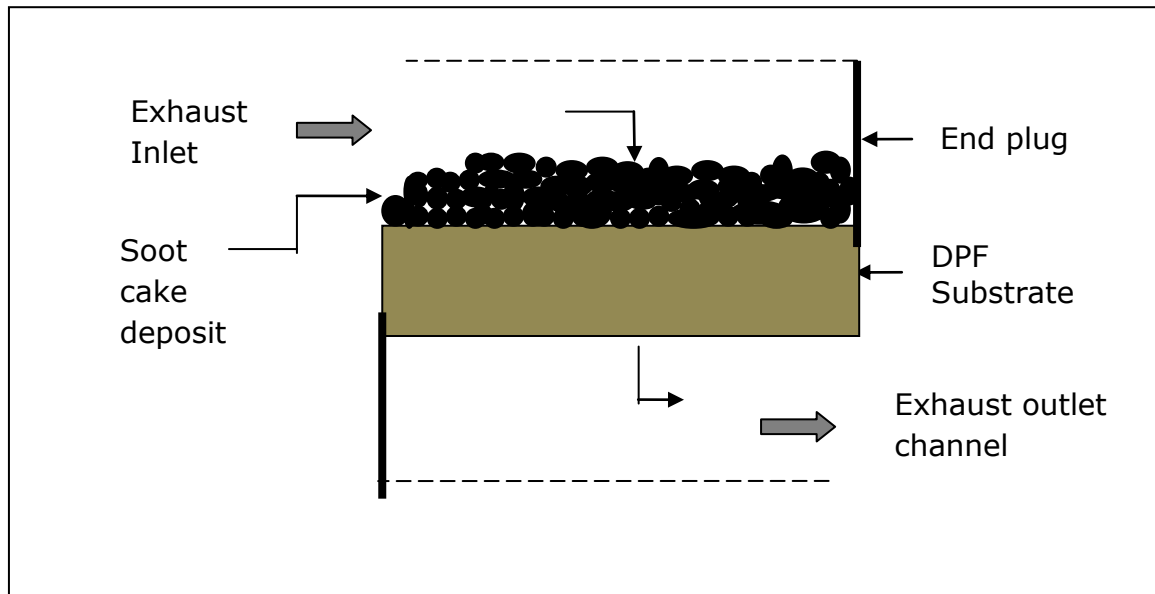


**Fig 2.2:** Schematic diagram of a DPF channel, adapted from reference (1)

## 2.2 Regeneration in a Diesel Particulate Filter

As PM loading increases, so does the back pressure. High back pressure is not desirable as it causes a fuel penalty as explained in reference (3). PM accumulation also needs to be limited as it causes excessive temperatures not experienced using active regeneration. At a certain load of accumulation of PM, the PM is oxidized to avoid these issues. There are two ways to categorize the mechanism for PM regeneration:

1. Active Regeneration
2. Passive Oxidation

During active regeneration, the PM is burned in the presence of oxygen. The inlet temperature to the DPF needs to be increased as the PM oxidizes only at higher temperatures ( $\geq 550$  °C). This temperature increase is accomplished by using external means. There are many ways to increase the DPF inlet gas temperature (4). One way to do this is by diesel fuel injection into the exhaust, upstream of a Diesel Oxidation Catalyst (DOC). As a result, there is a sizeable amount of hydrocarbon concentration entering the DOC. In the DOC, the hydrocarbons are oxidized thus increasing the exhaust temperature. The quantity of injected diesel is metered in order to achieve the

required DPF inlet temperature. Another way to achieve this is to use a fuel burner after the turbocharger to increase the temperature of the exhaust gas. Electrical and microwave heating are also considered as potential methods of DPF regeneration. The equations 2.1 and 2.2 show the active regeneration reactions (15).



Passive oxidation occurs via PM oxidation promoted by NO<sub>2</sub>. The temperature domain of passive oxidation is between 250 °C to 400 °C (1). In contrast, the light off temperature for active regeneration is generally around 550 °C. A lower light off temperature compared to the active regeneration is observed during passive oxidation as the rate of reaction with NO<sub>2</sub> is much greater than with O<sub>2</sub> even though NO<sub>2</sub> is present in lower concentrations (1). The equations 2.3 and 2.4 show the passive oxidation reactions (3).



The individual channels of a DPF are coated with a catalytic material known as a catalytic washcoat to reduce the activation energy required for the PM to oxidize (represented in Equations 2.1 through 2.4). The authors in (1 and 5) indicate that the catalytic washcoat provides sites where PM can come in contact with the catalyst. This increases the rate of PM oxidation. The catalyst itself is not consumed in the actual reaction. It only reduces the activation energy of the normal PM oxidation reaction. The catalyst formulation generally consists of precious metals such as platinum (Pt) or palladium (Pd). The contact of PM with the catalyst is a factor in determining how much the activation energy is reduced (1 and 5).

## 2.3 Pre-oxidation during regeneration

There have been studies of DPF active regeneration performance which have observed an unusually high rate of oxidation in a low temperature zone (under ~ 400 °C). This is consistent with the experimental data observed in this research. Darcy (6) observed this

phenomenon and attributed it to the presence of volatile organic fractions (VOFs) initially contained in the PM. The author suggests that the VOFs of PM burn (or decompose) simultaneously with the carbonaceous PM at temperatures below 450 °C.

Yezerets (7) investigated this initial high reactivity and observed PM oxidation below 350 °C. He concluded that it was not attributed to adsorbed HCs by basing this on a comparison of oxidation rates of fresh and pretreated PM in Temperature Programmed Desorption (TPD) studies. The presence of a DOC upstream of the DPF eliminates most of the HCs which would form the VOFs. The experiments performed by the authors determined that the low temperature high oxidation rate characteristics of particulate matter can be restored by exposure to ambient conditions for a considerable amount of time and this can be done repeatedly. The authors suggest that these changes in the oxidation characteristics of carbon are chemical in nature. According to this finding, the presence of VOFs in the PM is doubtful. Once this initial particulate pre-oxidation occurs, the remainder of the PM is uniformly oxidized and it is possible to define this oxidation by a set of Arrhenius kinetic parameters over a large range of temperature (~ 330° – 610 °C). Pre-oxidation was found to occur up to a maximum of 25% of PM conversion for some Temperature Programmed Oxidation (TPO) runs. The activation energies reported in this work for TPO runs of 2 different samples in the temperature range of 250 - 290 °C are 76 and 49 kJ/mol respectively. The corresponding activation energies are 126 and 146 kJ/mol respectively. These were observed by the authors in the temperature range of 330 - 610 °C

## **2.4 DPF Modeling Studies**

Studies on the kinetic modeling of PM oxidation during regeneration are reviewed in this subsection. The DPF oxidation model developed in references (1) through (4) is based on the 1-D, 2-layer model of Konstandapoulus et al. of reference (8), which is based on Bissett's work (9). This model used a 2-layer approach for the PM cake. Layer 1 (consisting of PM particles) was considered to be in contact with the catalyst. Thus catalytic oxidation was modeled to take place in layer 1. Layer 2 was where the non-catalytic PM oxidation was modeled to take place.

Premchand et al. in reference (10) improved this 1-D, 2-layer model to simulate active regeneration. This model also included

gaseous species oxidation and energy balance equations. The kinetic model for PM oxidation used in all the modeling work done in references (1) through (4) was a slightly modified form of the classical Arrhenius equation. This Arrhenius equation form is shown in Equation 2.5.

$$K = AT^n e^{E_a/RT} \quad \dots \dots \dots (2.5)$$

Where,  
 K = rate of oxidation  
 A = pre-exponential factor  
 E<sub>a</sub> = activation energy of oxidation  
 T = Temperature of exhaust  
 R = universal gas constant  
 n = order of reaction

Achour et al. in reference (11) used the classical Arrhenius form to model PM oxidation. They used a 'trigger law' or 'threshold law' to start the simulation of the oxidation process. The light off temperature, which is supposed to 'trigger' the PM oxidation, was fixed. Once this temperature is reached, the PM oxidation begins. Before that, the reaction rate is zero. This approach is not suitable to model the initial pre-oxidation of PM discussed in section 2.3, since the light off temperature of active regeneration is observed to be in the temperature region where pre-oxidation occurs (before 350 °C).

Neeft et al. in reference (12) discussed the relationship between active surface area and PM conversion for diesel fuel. With an increase in PM conversion the active surface area decreases and as a result the reaction rate also decreases. But, the authors mention that for PM, which is highly porous and reactive, the active surface area can does not decrease as a function of conversion. It increases due to factors like pore growth and occluded pore space opening as suggested by the authors. They derived a kinetic model for the PM depletion taking into consideration this important phenomenon. The effect of the partial pressure of oxygen in the gas phase is also considered in their model. This model form is shown in Equation 2.6.

$$K = K'_0 e^{E_a/RT} \quad \dots \dots \dots (2.6)$$

where,

$K$  = rate of oxidation

$K_0'$  = pre-exponential factor

$E_a$  = activation energy of oxidation

$T$  = Temperature of exhaust

$R$  = universal gas constant

The effect of partial pressure of oxygen and surface area is lumped in the pre-exponential factor as shown in Equation 2.7.

$$K_0' = c(1 - \xi)^{n_\xi} p_{O_2}^{n_{O_2}} \quad \dots \dots \dots (2.7)$$

$\xi$  = fraction of PM conversion.

$n_\xi$  = order of reaction

$p_{O_2}$  = oxygen partial pressure

$n_{O_2}$  = order of oxygen partial pressure

$c$  = constant based on surface area.

Darcy et al. in reference (6) used the work of Neeft (12) as the basis for their surface area based PM oxidation model. It has a modified version of the Arrhenius form. The classical Arrhenius rate form is multiplied by the mole fraction of oxygen and an order of PM retention. This form is shown in Equation 2.8. The pre-oxidation discussed in section 2.3 has also been modeled using a similar Arrhenius equation for VOF mass. The total oxidation is the addition of the two. The results reported showed that the PM oxidation is dependent on the PM conversion and as a result on the specific surface area.

$$K = Ae^{\frac{E_a}{RT}} (x_{O_2})^a m_0 \left[ \frac{m}{m_0} \right]^\beta \quad \dots \dots \dots (2.8)$$

where,

$K$  = rate of oxidation

$A$  = pre-exponential factor

$E_a$  = activation energy of oxidation

$R$  = universal gas constant

$x_{O_2}$  = mole fractions of oxygen

$T$  = Temperature of exhaust

$\alpha$  = order of O<sub>2</sub> mole fractions  
 $\beta$  = order of PM retention  
 $m_0$  = initial mass on filter  
 $m$  = instantaneous mass on filter

Activation energy for non-catalyzed PM oxidation reported by the authors in (6) is in the range of 160-165 kJ/mol. Activation energy equal to 114 kJ/mol was reported for the catalyzed PM oxidation. The range of activation energy values have been reported in the range of 140 -170 kJ/mol as cited in an extensive review of PM oxidation experiments and modeling by Stanmore et al. (13). Authors in (12) reported the activation energy of PM oxidation as 168 kJ/mol for non-catalyzed PM oxidation. Prasad and Bella in reference (16) studied the PM oxidation in a mini batch reactor and reported the value of activation energy as 160 kJ/mol. The activation energy values reported in the above references are listed in the Table 2.1.

**Table 2.1**  
 List of reported activation energies

Reference	E <sub>a</sub> (kJ/mol)	
	Non-Catalytic	Catalytic
6	160 - 165	114
12	168	
13	140-170	
16	160	

### **3. ACTIVE REGENERATION MODEL DESCRIPTION**

This chapter describes the assumptions, hypothesis, reactions and differential equations of the kinetic model used in this thesis. The model form was derived from references (6) and (12) since the trends observed in the experimental data are similar to those references.

As discussed in Section 2.3, references (6) and (7) described pre-oxidation occurring at temperatures lower than  $\sim 350$  °C. The change in reactivity was proposed to be chemical in nature and not morphological. In the experimental data observed in this research, pre-oxidation is found to occur until  $\sim 400$  °C, thus the same chemical dependency will be used to explain it.

#### **3.1 'Two soot' Hypothesis**

It is hypothesized in this research that there are two different types of PM oxidation processes occurring during active regeneration:

1. Pre-oxidation (under  $\sim 425$  °C)
2. Regular oxidation (425 - 650 °C)

The PM loaded on the filter can be subdivided based on these two types of oxidation. The portion of PM which takes part in pre-oxidation is called the *low activation energy PM* (LE PM). It oxidizes before 425 °C. The second type is called *high activation energy PM* (HE PM) since it oxidizes at high temperatures.

In the catalytic DPF, some portion of the total PM is assumed to take part in catalytic oxidation. This amount of PM is assumed to be in contact with catalyst. The remaining 'non-catalytic' PM is subdivided according to the 'two soot' hypothesis. The subsections 3.1.1 and 3.1.2 describe this hypothesis for non-catalyzed and catalyzed samples respectively.

No portion of the LE PM is assumed to be in contact with the catalyst. This is based on observing the experimental data for the catalyzed samples and comparing it to that of the non-catalyzed samples of the same substrate. The LE PM is observed to oxidize until  $\sim 425$  °C in the absence of catalyst. Hence, if some portion of it was in contact with the catalyst, the rate of pre-oxidation would be faster for

the catalyzed samples of the same substrate. But it was observed from experimental data that faster pre-oxidation does not occur for catalyzed samples. Furthermore, the difference between the masses of the catalyzed and non-catalyzed samples at 350 °C is less than 0.5% of total mass. This assumption reduces the complexity of the model by reducing the number of parameters to be estimated.

### 3.1.1 Non-catalyzed DPF

PM loaded on the non-catalyzed DPF wall is of the two types mentioned in the hypothesis in Section 3.1. In the Figure 3.1 the schematic representation of a single channel of a non-catalyzed DPF is shown.

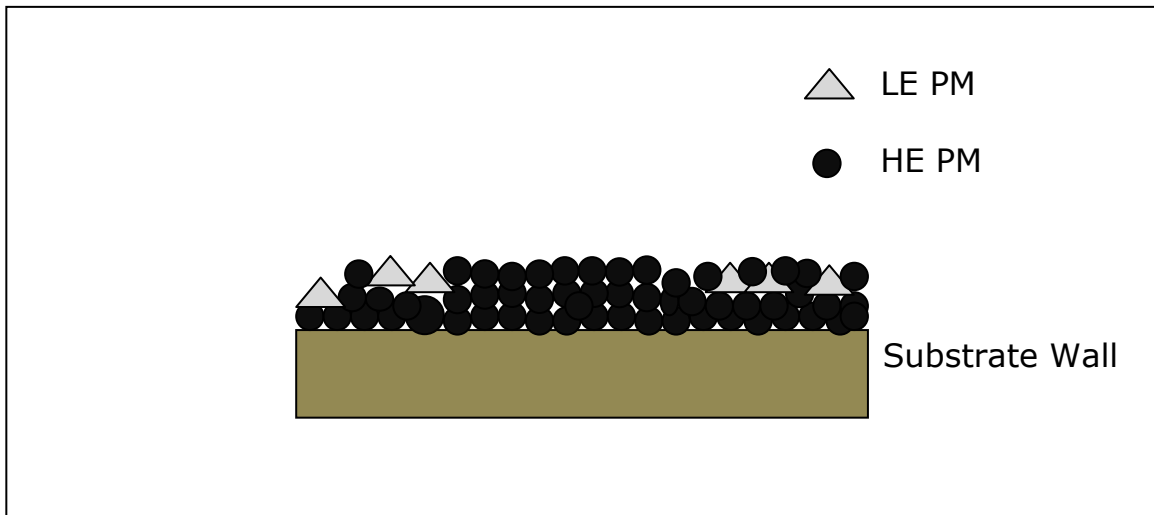


**Fig 3.1:** Schematic diagram of PM types on the wall of a non-catalyzed DPF



### 3.1.2 Catalyzed DPF

Due to the presence of the catalyst, some part of the HE PM is in contact with the catalyst surface. This PM burns at a lower temperature than the HE PM not in contact with the catalyst. Hence this PM is called 'catalyzed PM' (CT PM). In Figure 3.2 the schematic representation of a single channel of a catalyzed DPF is shown. As per the assumption in Section 3.1, the LE PM is not shown in contact with the catalyst.

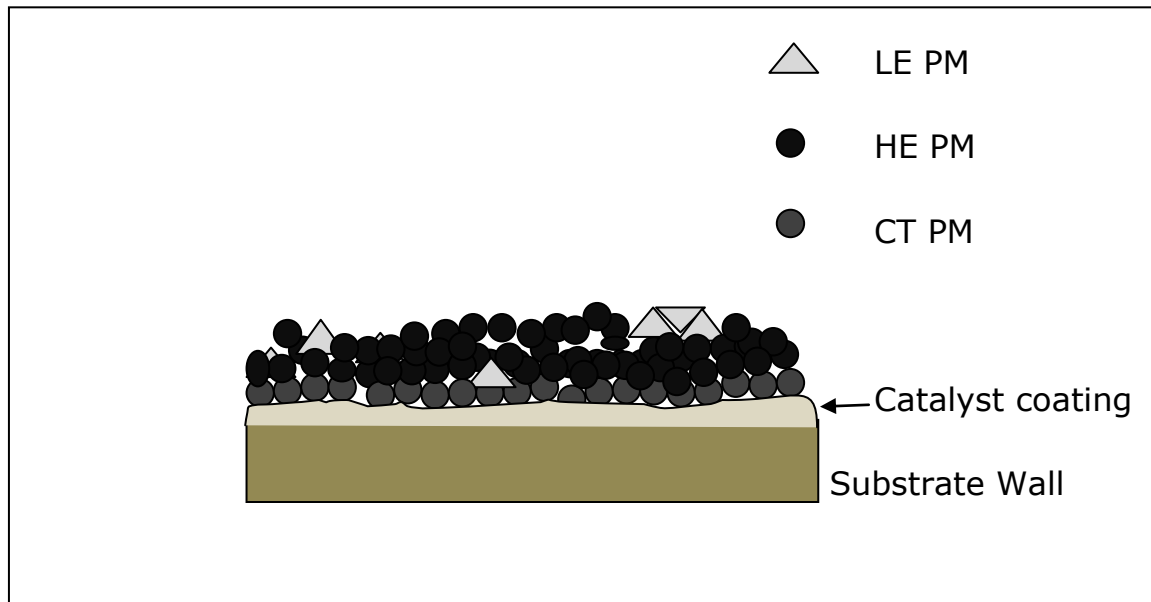


**Fig 3.2:** Schematic diagram of PM types on the wall of a catalyzed DPF

## 3.2 DPF PM Oxidation Model Assumptions

The model developed for this research was a zero dimensional model. It simulates only the depletion of PM mass from a pre-loaded filter. The model was developed in MATLAB/Simulink<sup>®</sup> based on the assumptions made below:

1. Exhaust gas is considered to be an ideal gas.
2. A single square channel is considered representative of all the DPF channels.
3. Radial variation of the exhaust flow, gaseous concentrations and temperature is neglected.

4. Flow through the filter is considered to be laminar.
5. PM oxidation reaction rates follow a modified Arrhenius form.
6. Heat transfer to the ambient is neglected.
7. Partial pressure of oxygen in the gas phase in the DPF is assumed to be constant.
8. Mass retained in the filter does not vary axially or radially.

### 3.3 DPF PM Oxidation Kinetic Model

This section explains the kinetic model including the reactions and differential equations.

#### 3.3.1 Inputs to the model

The initial mass of PM, temperature of the exhaust gas and the kinetic parameters are the inputs to the model. Evolution of the mass of PM on the filter is determined from the space velocity of the exhaust gas and the total amount of carbon monoxide and carbon dioxide recorded in the experimental data. Here it is assumed that the mass retained on the filter at the end of the experiment is exactly zero. Thus the summation of the total mass of carbon extracted from the amounts of CO and CO<sub>2</sub> is the mass of PM present on the filter before the start of regeneration denoted as  $m_0$ . The temperature of exhaust gas recorded in the experiment is used for calculating the reaction rates in the model.

#### 3.3.2 Equations of the Model

Carbon dioxide (CO<sub>2</sub>) is formed as the product of active regeneration. In a non-catalyzed DPF, carbon monoxide (CO) can be formed due to depletion of oxygen in the reaction zone. In catalyzed DPF samples, complete conversion to CO<sub>2</sub> is observed. The C in the reactions refers to carbon black or PM (15).



The rate equation for the depletion of the PM mass is derived from references (6) and (12) and is shown in Equation 3.3, where subscript j denotes the type of PM. The rate of depletion of PM from the filter is based on the Arrhenius form and the amount of PM in the filter. The partial pressure of oxygen is assumed to be constant. The O<sub>2</sub> mole fraction term in the form used in (6) is lumped with the term A<sub>j</sub> in equation 3.3. Its order is assumed to be one for simplicity of the model form. Values close to one have been cited in references (12) and (13).

$$\dot{m}_j(t) = f(t, m_j(t)) = -A_j e^{\left(\frac{-E_j}{RT}\right)} m_{0,j} \left[ \frac{m_j(t)}{m_{0,j}} \right]^{\beta_j} \quad \dots \dots \dots (3.3)$$

$$\int_{t_0}^{t_f} \dot{m}_j(t) dt = \int_{t_0}^{t_f} -A_j e^{\left(\frac{-E_j}{RT}\right)} m_{0,j} \left[ \frac{m_j(t)}{m_{0,j}} \right]^{\beta_j} dt$$

where  $m_j(0) = m_{0,j}$  and  
j represents the type of PM (LE, HE or CT)

The mass is integrated over time as shown in Equation 3.4.

$$m_j(t_f) = m_j(t_0) + \int_{t_0}^{t_f} -A_j e^{\left(\frac{-E_j}{RT}\right)} m_{0,j} \left( \frac{m_j}{m_{0,j}} \right)^{\beta_j} dt \quad \dots \dots \dots (3.4)$$

Using Euler integration, the discrete mass update equation is shown in Equation 3.5.

$$m_{k+1,j} = m_{k,j} + hf(t, m_{k,j}) \quad \dots \dots \dots (3.5)$$

The rate equations are of degree of PM retention ( $m_j/m_{0,j}$ ) dependent

Arrhenius form. The pre-exponential  $A_j$  is lumped as it includes the mole fractions of  $O_2$ .

$k$  represents the time

$A_j$  = lumped pre-exponential factor in  $s^{-1}$

$E_j$  = activation energy in  $kJ/mol$

$m$  = mass of PM is in grams.

$R$  = Universal gas constant ( $m^2 kg s^{-2} K^{-1} mol^{-1}$ )

$T$  = Inlet Temperature of gas (K)

$\beta$  = order of PM retention degree. Higher the value of  $\beta$ , lesser is the dependence on the degree of PM retention.

$t_0$  = starting time

$t_f$  = finish time

$m$  = time step

The instantaneous mass on the filter is given by Equation 3.6. The subscripts l, h and c stand for LE, HE and CT PM respectively.

$$m_i = \sum m_{i,j} \quad \dots \dots \dots (3.6)$$

where  $j = l, h$  or  $c$

The masses  $m_{0,l}$ ,  $m_{0,h}$ ,  $m_{0,c}$  are assumed to be fractions of  $m_0$ .

$$m_{0,l} = \theta \lambda m_0 \quad \dots \dots \dots (3.7)$$

$$m_{0,h} = (1-\theta) \lambda m_0 \quad \dots \dots \dots (3.8)$$

$$m_{0,c} = (1-\lambda) m_0 \quad \dots \dots \dots (3.8)$$

where,

$\lambda$  = fraction of HE PM not in contact with the catalyst.

$\theta$  = fraction of LE PM in the amount of PM not in contact with the catalyst.

The schematic representation of this PM type assumption with respect to equations 3.7, 3.8, 3.9 is shown in figure 3.3.

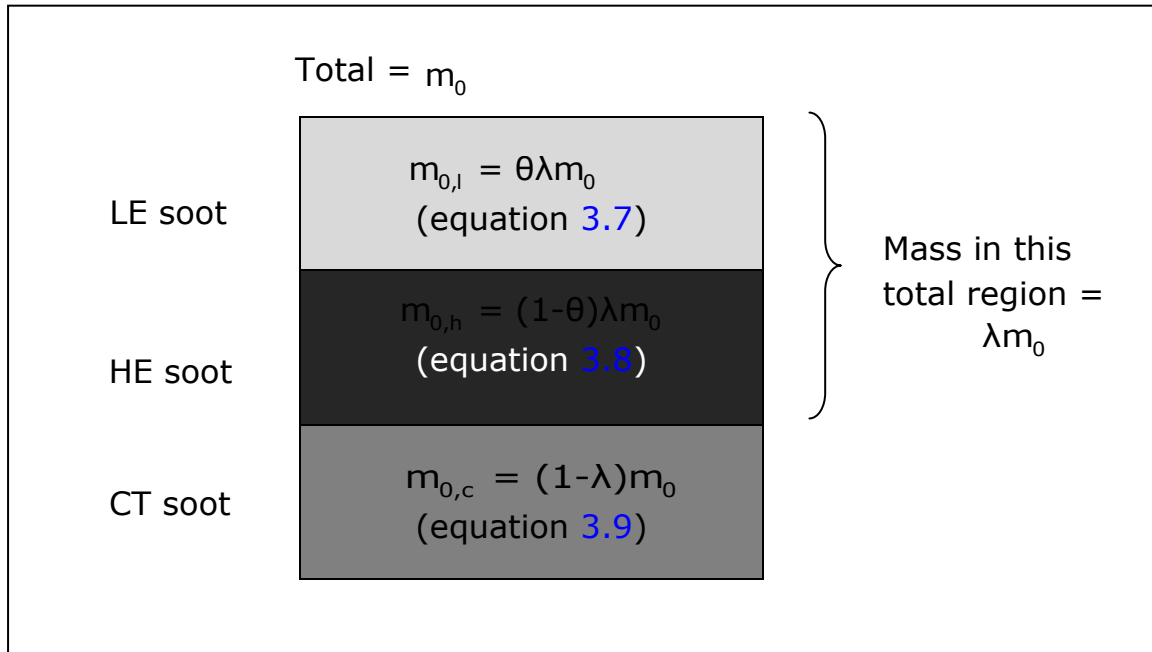


**Fig 3.3:** Schematic diagram of PM type distribution in a catalyzed DPF

The total amount of PM is divided into CT PM and 'non-CT' PM (HE and LE PM) by the fraction  $\lambda$ . For non-catalyzed samples  $\lambda = 1$  since there is no catalyst. The mass of PM which is not in contact with the catalyst is divided into LE and HE PM by the fraction  $\theta$ .

## **4. EXPERIMENTAL DATA ACQUISITION**

This section provides a brief description of the experimental setup and the experiments that were carried out in order to provide data for calibrating the model described in Chapter 3. The data collection process can be defined in the following steps.

1. DPF mini filters were obtained by Navistar Inc.
2. PM loading of the mini filters was done by Exova Ltd. On these mini filters.
3. PM loaded filters were shipped in dry ice to Oak Ridge National Labs (ORNL).
4. Active regeneration experiments were performed at ORNL

### **4.1 PM Loading Experiment**

The DPF mini cores (1 inch O.D X 3 inches in length) were loaded with PM at Exova. The setup consisted of a Navistar prototype MaxxForce® 13 liter diesel engine with 0.5 g NO<sub>x</sub> out. Loading of the mini DPFs was performed at an engine condition with a high exhaust gas PM density in order to provide the fastest possible loading rate. This condition was 1950 rpm, 350 lb/ft, and was defined based on PM engine map data. The fuel used in the engine was Ultra Low Sulfur Diesel (ULSD).

In order to accelerate the loading rate further, the EGR level at the engine test condition was manually increased in order to raise the exhaust gas PM level. Running at this condition, a raw sample of exhaust gas was drawn through a sampling system so that the particulate was deposited on the mini filters. The mini filters were mounted within an oven (heated box) in the sampling system and a heated sample line was used in order to maintain high exhaust gas temperatures to ensure that the PM was similar to that deposited on a production DPF. During the test, the smoke meter was regularly checked and the EGR was adjusted to maintain smoke meter reading at a consistent level. It was also important to maintain the realistic PM composition to be able to accurately calculate the loading time required for different PM loading levels. This was done based on a known PM mass flow rate at the test condition and the volumetric rate through the sampling system.

The Figure 4.1 shows the mini filter and its dimensions a.



**Fig 4.1:** Photograph of one of the mini DPF cores and holder

Figure 4.2 shows the layout of the sampling system.

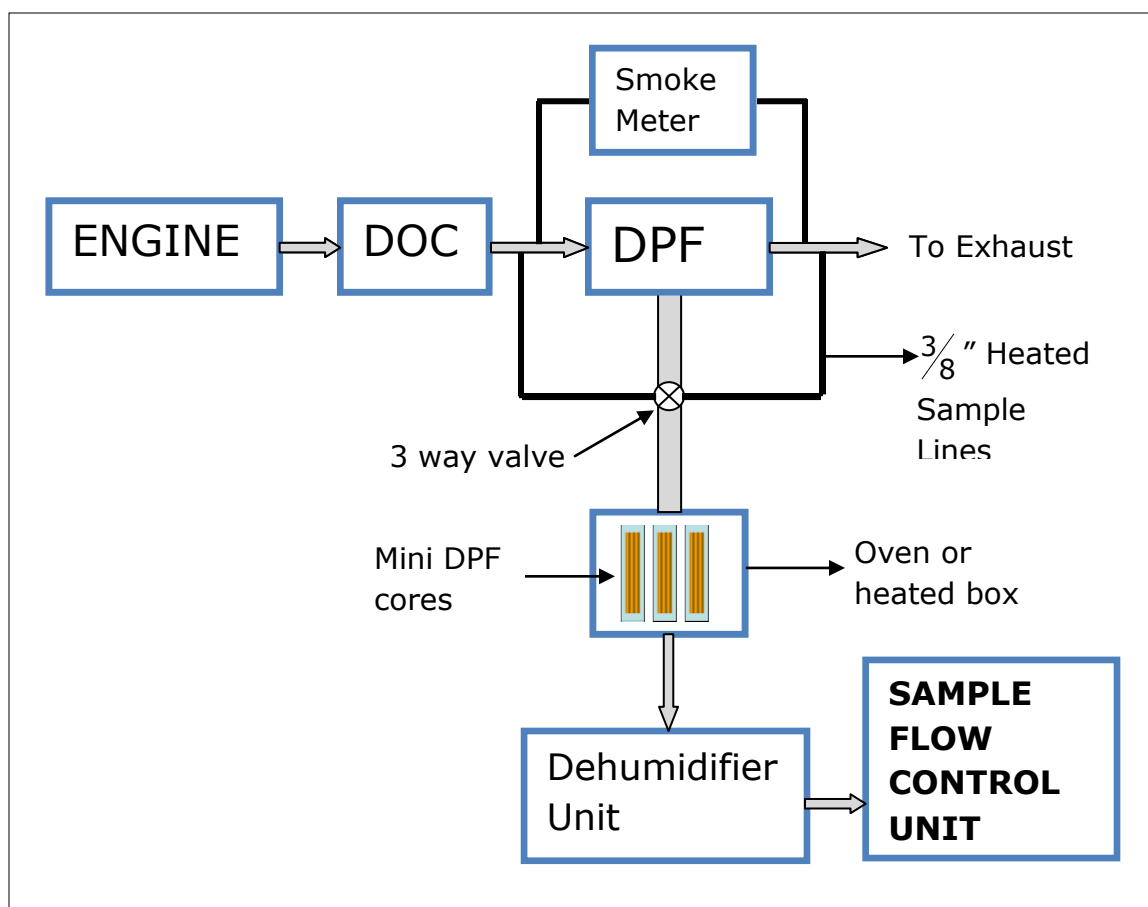


**Fig 4.2:** Experimental Layout (PM Sampling System)

## 4.2 Active Regeneration Experiment

The mini DPFs loaded at Exova were shipped in dry ice and stored in a freezer at ORNL. The data used for modeling was from 6 different formulations. It included three samples each of non-catalyzed cordierite, aluminum titanate and silicon carbide and 3 samples each of catalyzed cordierite, aluminum titanate and silicon carbide.

All experiments were run on an automated flow reactor that used synthetic gas mixtures, electric furnaces to heat the sample and inlet gases, and a high speed MKS Instruments Multigas 2030HS Fourier Transform Infra Red (FTIR) spectrometer for outlet gas composition measurements (including CO, CO<sub>2</sub>, H<sub>2</sub>O, NO, NO<sub>2</sub>, N<sub>2</sub>O, and selected hydrocarbon species).

Temperature Programmed Oxidation (TPO) was performed on the samples to achieve the burnout. The gas composition for the TPO experiment included 10% O<sub>2</sub> and 5% H<sub>2</sub>O.

### 4.2.1 Protocol of the experiment

All runs were conducted at a space velocity of 40000 hr<sup>-1</sup> based on total filter volume and flows at standard temperature (0 °C) and pressure (1 atm). All experiments began with a short bypass run during which the inlet gases were sent directly to the analytical instrumentation to ensure accurate instrument calibration and correct system operation. Upon completion of the bypass measurement, filter sample heating commenced under a flow of N<sub>2</sub> only. Once the filter temperature reached 100 °C, 5% H<sub>2</sub>O was added to the flow. After the filter temperature stabilized at 200 °C, the reactive gas O<sub>2</sub> flows were initiated and the filter temperature was linearly increased to 600 °C at a rate of 2 °C/min. At the conclusion of the temperature ramp, the filter temperature was held at 650 °C for 10 minutes to ensure complete filter regeneration. The protocol followed for these experiments can be summarized in 4 steps:

1. Stabilize the DPF temperature at 200 °C.
2. Stabilize the flow of gas at 40000 hr<sup>-1</sup> space velocity.
3. Begin the flow of oxidant (10% O<sub>2</sub>).
4. Ramp the temperature to 650°C at 2 °C/min.



### 4.2.2 Layout of the reactor

Figure 4.4 shows the layout of the reactor. The miniature (1 inch O.D X 3 inches in length) particulate filters were loaded in a 1.26 inch outer diameter quartz tube. The tube was modified to create a slight pinch just downstream of the desired filter position to prevent the gas from pushing the filter inside the tube. Strands of ceramic fiber insulation (pretreated in air at 600 °C) were wrapped around the outside of the filter to form a seal between the filter and the inside wall of the quartz tube. The upstream portion of the reactor tube was filled with a bed of 3 mm diameter quartz chips to ensure a uniform inlet gas temperature. The tube was fitted with custom stainless steel end caps fabricated from Swagelok components. The end caps contained multiple entry/exit ports for connection of gas lines, thermocouples, and pressure transducers. The end caps were sealed to the quartz reactor tube with graphite ferrules.

The quartz reactor tube was enclosed in a Lindberg/Blue M Mini-Mite tube furnace. The 6.4 mm diameter stainless steel reactor gas lines were maintained between 180 and 200 °C to minimize gas adsorption and vapor condensation with heat tapes (Cole Parmer EW-36050-10) controlled by variable voltage transformers. The inlet gas line was heated to the desired catalyst operating temperature using a cylindrical heating element (Omega Engineering CRFC-36/115-A) and heat tape, both controlled by Yokogawa UP150 temperature controllers. The heat tape on the reactor outlet gas line was also controlled with a UP150 temperature controller. Thermocouples (0.5 mm diameter type K, Omega Engineering Inc.) were placed 5 mm upstream of the filter, in the axial midpoint of an outlet channel located near the radial filter center, and 5 mm downstream of the filter. System pressures were monitored with Omega Engineering Model PX419-030AV pressure transducers. A differential pressure transducer (Omega Engineering Model PX419-005DWU5V) was used to measure the pressure drop across the filter. Synthetic exhaust gas mixtures were generated from compressed gas sources through the use of mass flow controllers (MKS Instruments Model 1479A). Nitrogen was supplied from a cryogenic liquid nitrogen Dewar. All other gases were drawn from gas bottles (Air Liquide America Specialty Gases LLC, Alphagaz 1 or better purity). Water was introduced with an HPLC pump (Eldex Laboratories Optos 1LMP) and a custom vaporization system.

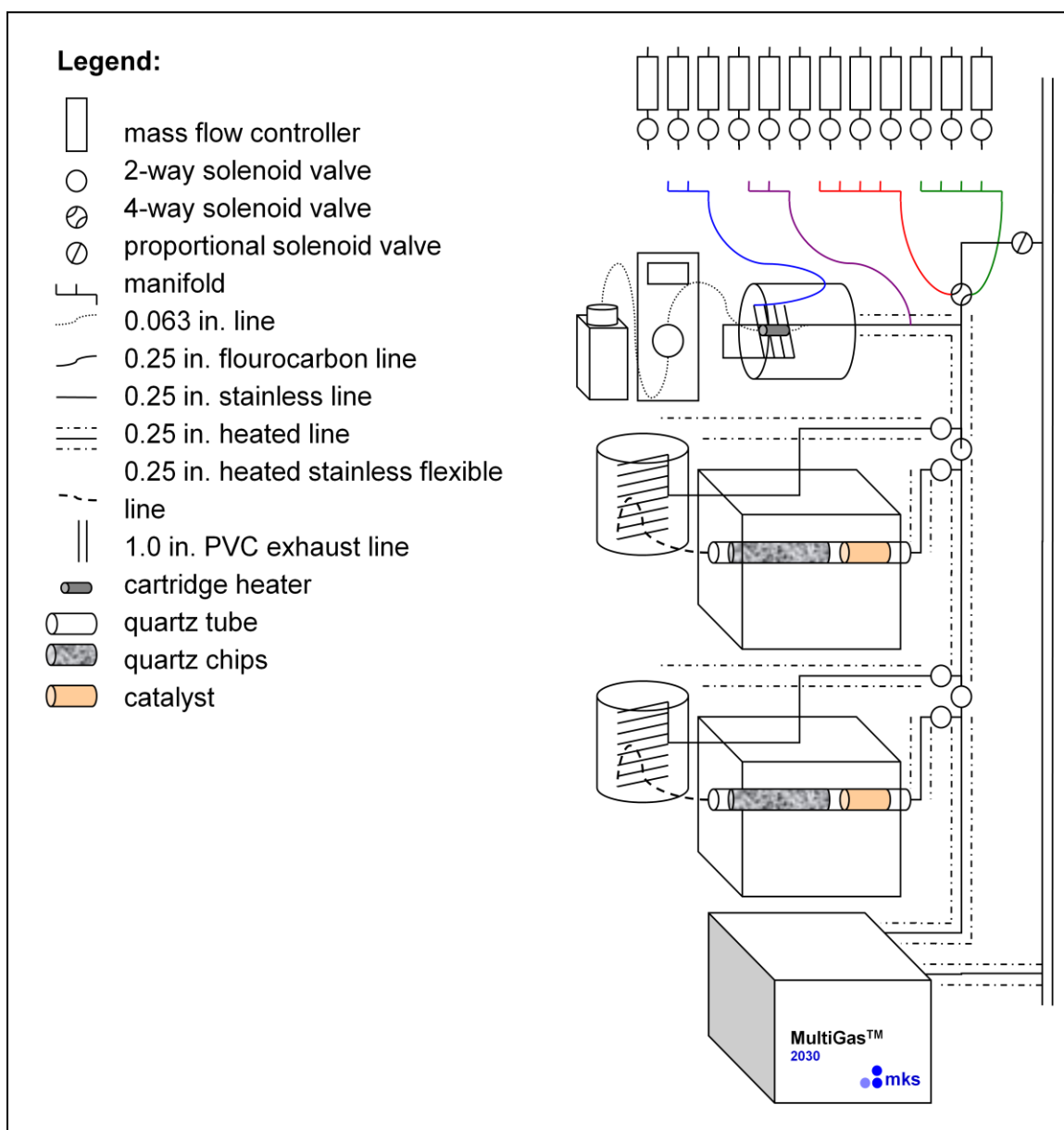


**Fig 4.3:** *Layout of the reactor*

Equivalence ratio was measured with a prototype NO<sub>x</sub>/O<sub>2</sub> sensor provided by Navistar. All other gas species were measured with an MKS Instruments Multigas 2030HS FTIR spectrometer. Data acquisition and instrument communication were accomplished with National Instruments hardware, including: m-series analog output (PCI-6703) and multifunction input/output (PCI-6225) PCI cards; SCXI signal conditioning modules and terminal blocks (SCXI-1102, TC-2095); a USB/RS485 converter (USB-485); and a USB/CAN adaptor

(USB-8473). A custom National Instruments LabVIEW program provided automated system control and data logging.

## 5. RESULTS AND DISCUSSION

This chapter provides an analysis of the experimental data used for model calibration. The kinetic parameter optimization results of model calibration are discussed. The test data was obtained as explained in Section 4.

### 5.1 Experimental Data Analysis

The PM oxidation tests were carried out at ORNL using six DPF mini filters were used for oxidation –

1. Cordierite – Washcoated and non-washcoated
2. Aluminum Titanate - Washcoated and non-washcoated
3. Silicon Carbide - Washcoated and non-washcoated

The PM loading for all the DPF mini filters was 7 g/l. This PM was subsequently oxidized during the TPO and the concentration of gases, temperature and pressure was recorded. Space velocity and the CO and CO<sub>2</sub> time histories were used to determine the experimental rate of PM oxidation. By using this formula, the experimental rate was calculated in g/s. Experimental mass profiles were plotted based on this rate of oxidation using Euler integration. This is shown in Equation 5.1.

$$m_{k+1,j} = m_{k,j} + hf(t, m_{k,j}) \quad \dots \dots \dots (5.1)$$

where,

m is the actual mass of PM

h = 1 sec

k represents time in seconds and

j represents PM type (LE, HE, CT)

f(t, m<sub>k,j</sub>) = rate of oxidation per second calculated from experimental data (g/s). This is shown below in equation 5.2.

$$f(t, m_{k,j}) = \underbrace{\frac{(MW_C)(ppm2mol)}{n}}_{\text{Convert to g/l}} \times \underbrace{\frac{(SV)(Vol_{DPF})}{3600}}_{\text{Convert to l/s}} \times 1000 \times G_j \quad \dots \dots \dots (5.2)$$

where,

$MW_C$  = Molecular weight of C

ppm2mol = Conversion of ppm to mole fractions

$n$  = 22.4 liters (1 mole of ideal gas at STP)

SV = Space velocity in 1/hr

$Vol_{DPF}$  = Volume of mini DPF core

$G_j$  = Experimental values of CO + CO<sub>2</sub> at time instant  $j$  in ppm

The actual mass of PM ( $m$ ) is calculated from by summing the rate vector. It is assumed that mass retained on the filter at the end of regeneration is 0. This calculated value is different from the value observed at the Exova filter weighing facility. Since the mini DPFs were shipped from Exova to ORNL, there is a possibility of loss.

The comparison of the calculated PM mass and observed PM mass is shown in Table 5.1.

**Table 5.1**  
Mass of PM loading

Sample		Calculated from ORNL data (g)	Weighed at Exova (g)
Material	Catalyzed		
Cordierite	No	0.2626	0.2892
Aluminum Titanate	No	0.3103	0.2772
Silicon Carbide	No	0.2714	0.2791
Cordierite	Yes	0.2551	0.2612
Aluminum Titanate	Yes	0.2442	0.2759
Silicon Carbide	Yes	0.2929	0.2870

### 5.1.1 Non-Catalyzed DPF Data Analysis

One of the findings from the experimental data was that the substrate material does not affect the PM oxidation kinetics. This can be seen in Figures 5.1 and 5.2. Figure 5.1 compares the actual rate of oxidation of the 3 non-catalyzed substrates. Some pre-oxidation (discussed in section 2.3) is observed under 425 °C for all the substrates which is captured in the model form corresponding to LE PM. The Equation 3.3 represents the model form.

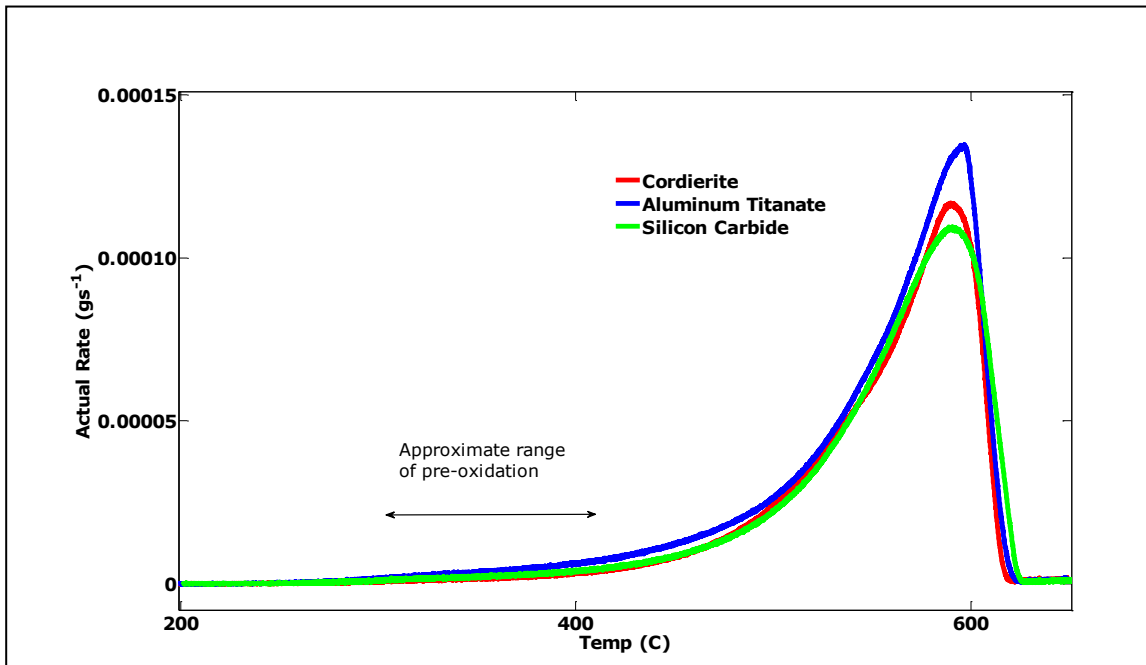


**Fig 5.1:** Actual rate of PM oxidation for 3 different non-catalyzed substrates

The initial mass present in the three substrates is different. The actual rates are divided by the initial mass to obtain the normalized rates. The rate of oxidation peaks at about 590 °C. The comparison of the normalized rates can be seen in Figure 5.2. The cordierite sample has the highest peak at  $0.00045 \text{ s}^{-1}$ . The aluminum titanate sample has a peak at  $0.00044 \text{ s}^{-1}$  which is 2% lesser than the cordierite sample. The silicon carbide sample has a peak at  $0.0004 \text{ s}^{-1}$  which is 11% lesser than the cordierite sample.

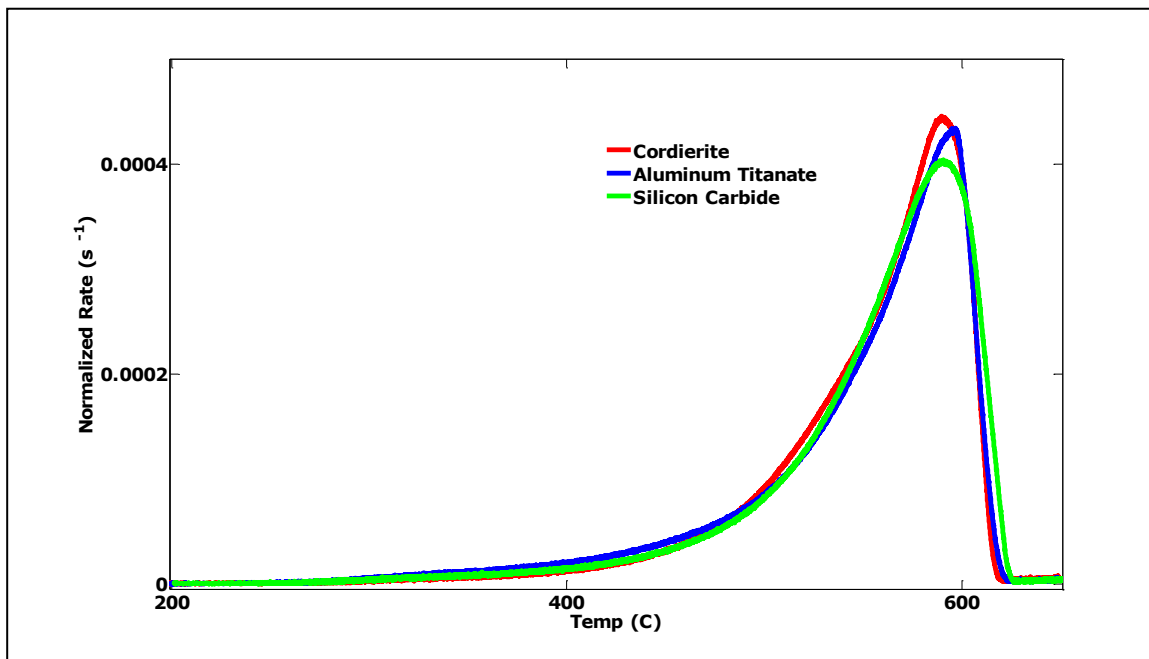
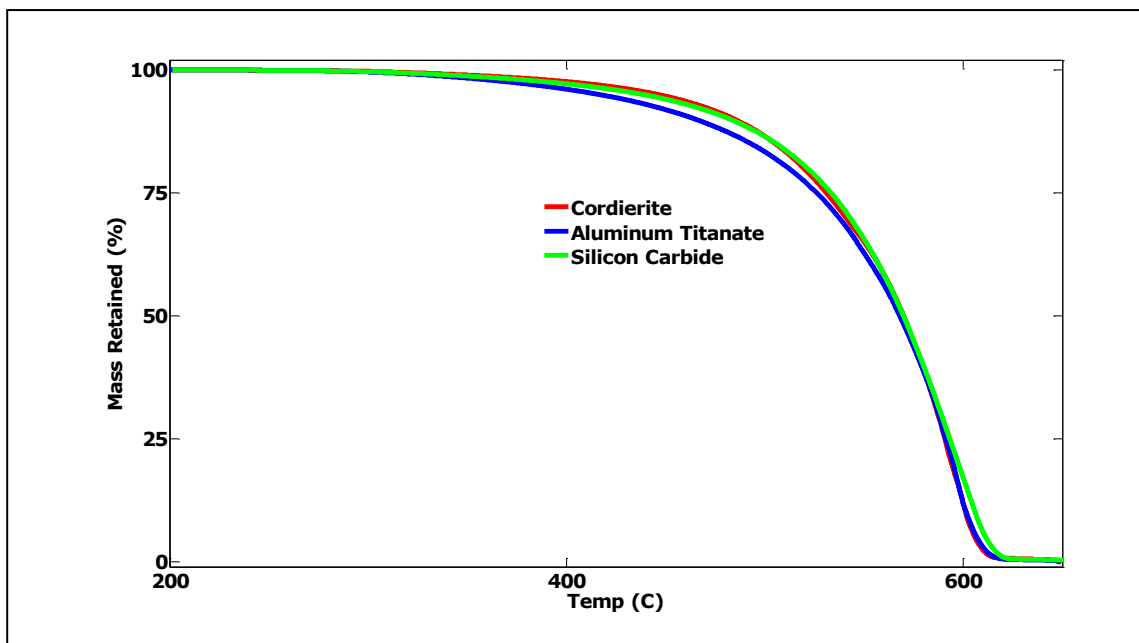


**Fig 5.2:** Normalized rate of PM oxidation for 3 different non-catalyzed substrates

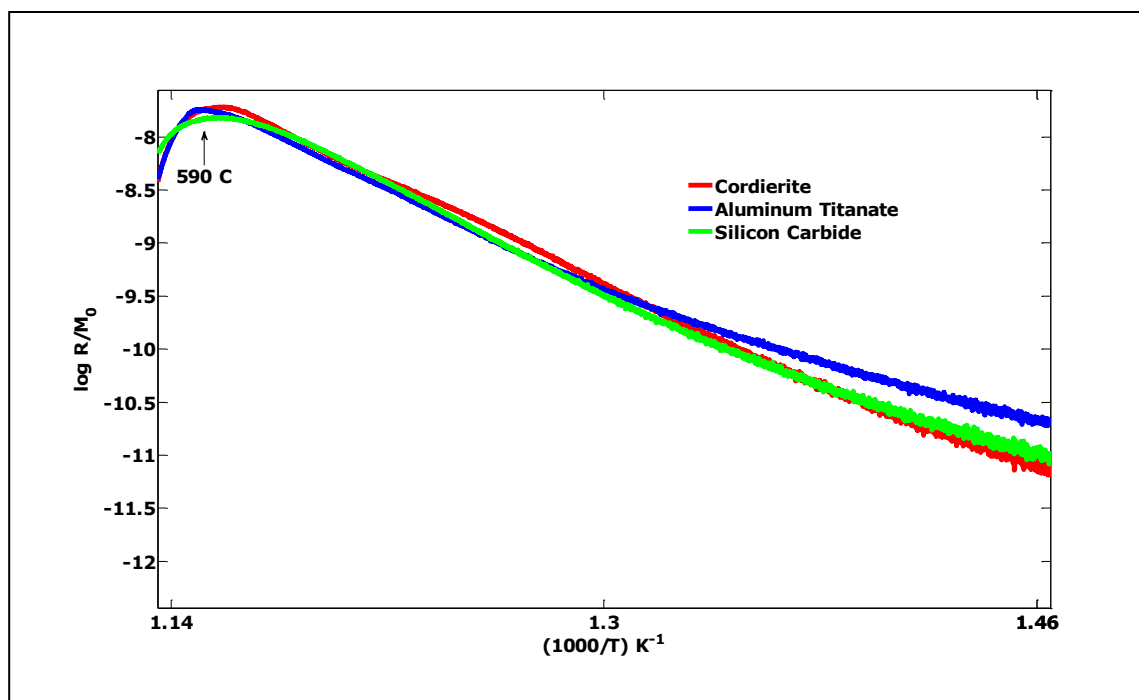
The aluminum titanate sample shows more pre-oxidation than the other two samples. The amount of pre-oxidation occurring in the cordierite and silicon carbide samples is about 6 % of the initial mass whereas that for the aluminum titanate is approximately 8 % of the initial mass on the filter. This can be observed in the temperature region below approximately 425 °C in Figure 5.3.

Figure 5.3 shows the normalized mass for the three samples. The HE PM oxidation characteristics (above temperature  $\sim 480$  °C) are very similar for all the samples clearly proving that HE oxidation is substrate independent.

Figure 5.4 shows the Arrhenius plot of the experimentally calculated rate. It is linear till about 590 °C. After that it curves downwards.



**Fig 5.3:** Normalized mass retained for three different non-catalyzed substrates



**Fig 5.4:** Experimental Arrhenius Plot for three different non-catalyzed substrates



An attempt was made to determine the values of  $\beta_j$  from the experimental data. We can write the Equation 3.3 shown below as Equation 5.3 when we take log of LHS and RHS.

$$\dot{m}_j(t) = f(t, m_j(t)) = -A_j e^{\left(\frac{-E_j}{RT}\right)} m_{0,j} \left[ \frac{m_j(t)}{m_{0,j}} \right]^{\beta_j} \quad \dots \dots \dots (3.3)$$

$$\ln \left[ \frac{\dot{m}_j(t)}{m_{0,j}} \right] = \ln \left\{ \underbrace{\left[ A_j e^{\left(\frac{-E_j}{RT}\right)} \right]}_K \left[ \frac{m_j(t)}{m_{0,j}} \right]^{\beta_j} \right\} \quad \dots \dots \dots (5.3)$$

Negative sign is dropped since it there only to indicate that the rate is that of removal of mass. Thus Equation 5.4 reduces to Equation 5.7

$$\ln \left[ \frac{\dot{m}_j(t)}{m_{0,j}} \right] = \ln(K) + \beta_j \ln \left[ \frac{m_j(t)}{m_{0,j}} \right] \quad \dots \dots \dots (5.4)$$

Thus  $\ln \left[ \frac{\dot{m}_j(t)}{m_{0,j}} \right]$  versus  $\ln \left[ \frac{m_j(t)}{m_{0,j}} \right]$  was plotted to determine  $\beta_j$ .

The value of the slope  $\beta_j$  is approximately 0.5 for approximately 75 – 100 % (585 - 610 °C range) of PM mass conversion range as seen in Figure 5.5.

$$\log \left[ \frac{R}{M_0} \right] \text{ denotes } \ln \left[ \frac{\dot{m}_j(t)}{m_{0,j}} \right]$$

$$\log \left[ \frac{M}{M_0} \right] \text{ denotes } \ln \left[ \frac{m_j(t)}{m_{0,j}} \right]$$

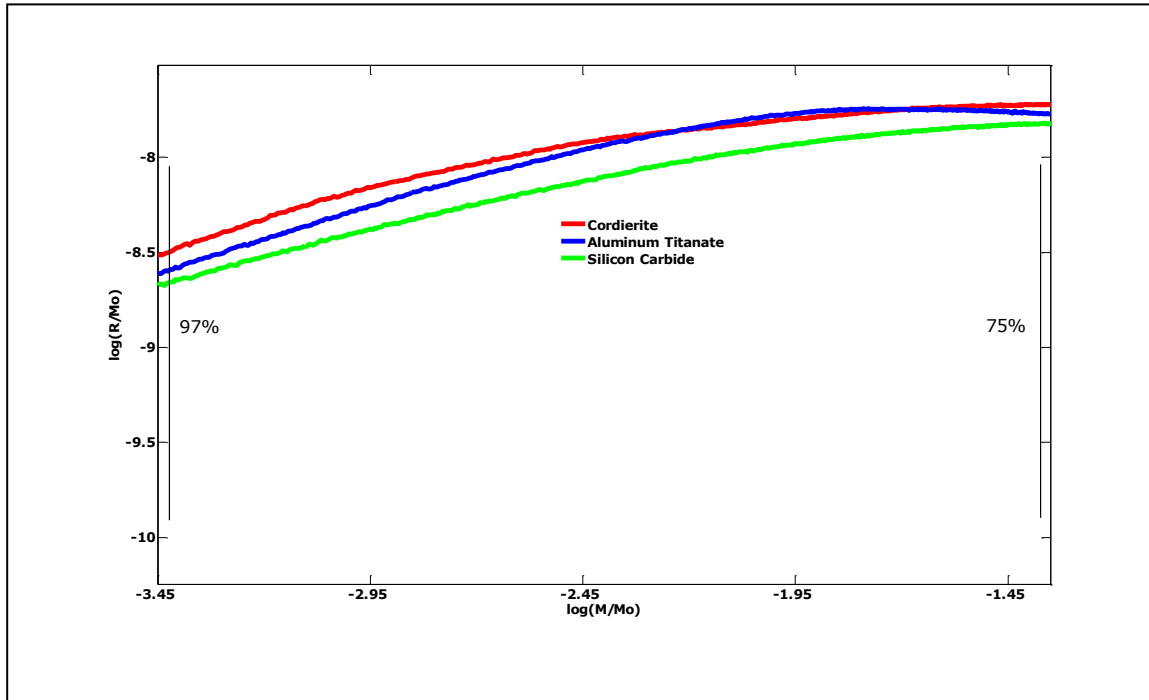


**Fig 5.5:** Calculation of  $\beta_h$  from experimental data (high conversion:  $\sim 75 - 100$  %)

The Figure 5.6 is a plot of  $\ln \left[ \frac{\dot{m}_j(t)}{m_{0,j}} \right]$  versus  $\ln \left[ \frac{m_j(t)}{m_{0,j}} \right]$  for the

conversion range of 15 – 75 %. The value of  $\beta_h$  during this range is roughly -1 for a major part. This suggests that the rate of oxidation is inversely proportional to the conversion. Results in (6 and 12) have reported values between 0.49 and 0.8. The Arrhenius plot in Figure 5.4 is linear in this region. Thus, it means that the order of reaction is close to 1.

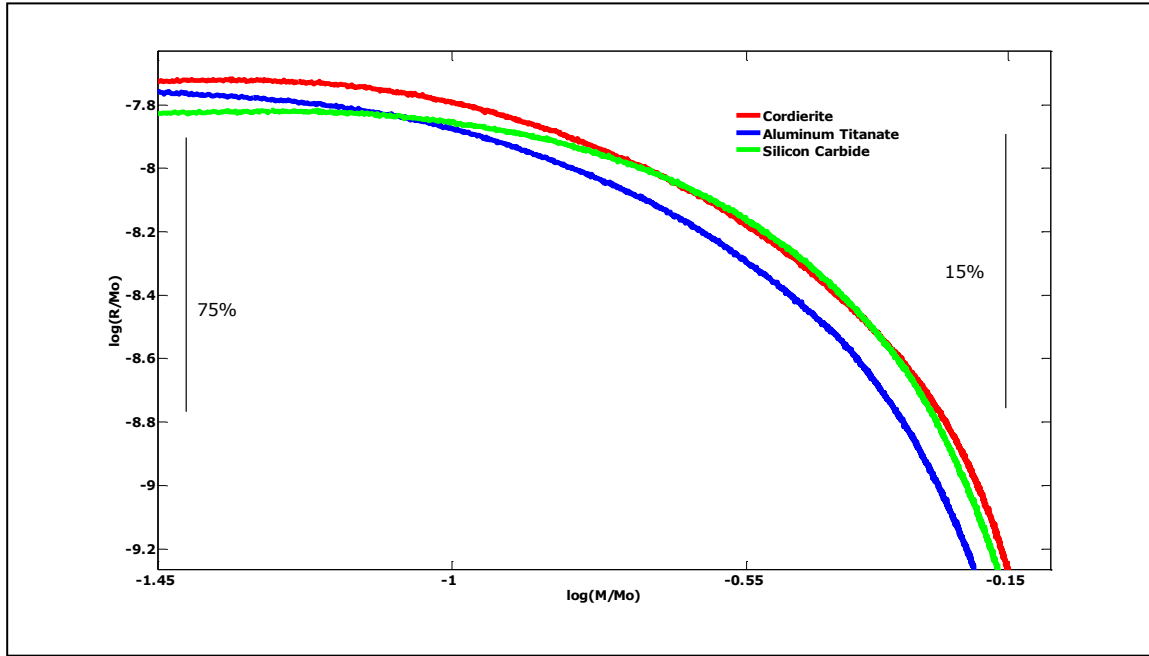


**Fig 5.6:** Calculation of  $\beta_h$  from experimental data (mid conversion:  $\sim 15 - 75\%$ )

The value of  $\beta_i$  for LE PM is not computed in similar fashion as the range of conversion in the pre-oxidation region (below 425 °C) is less than 10% of total mass. Thus the value of the term  $\frac{m_j(t)}{m_{0,j}}$  is very

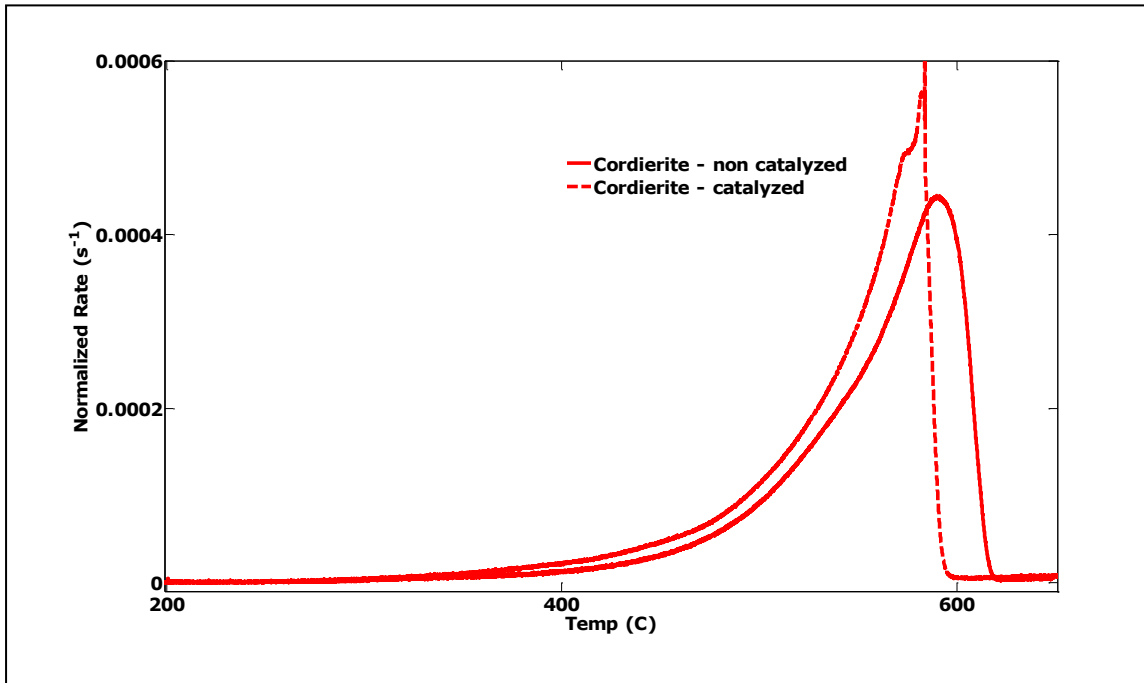
close to 1. As a result, its power does not have a significant impact.

The rate of depletion of the LE PM occurring at lower temperatures (below  $\sim 425$  C) is assumed to be of the classical Arrhenius form used in the references (11-14, 18). That is the order of reaction  $\beta_i$  is assumed to be 1. This simplifies the model.

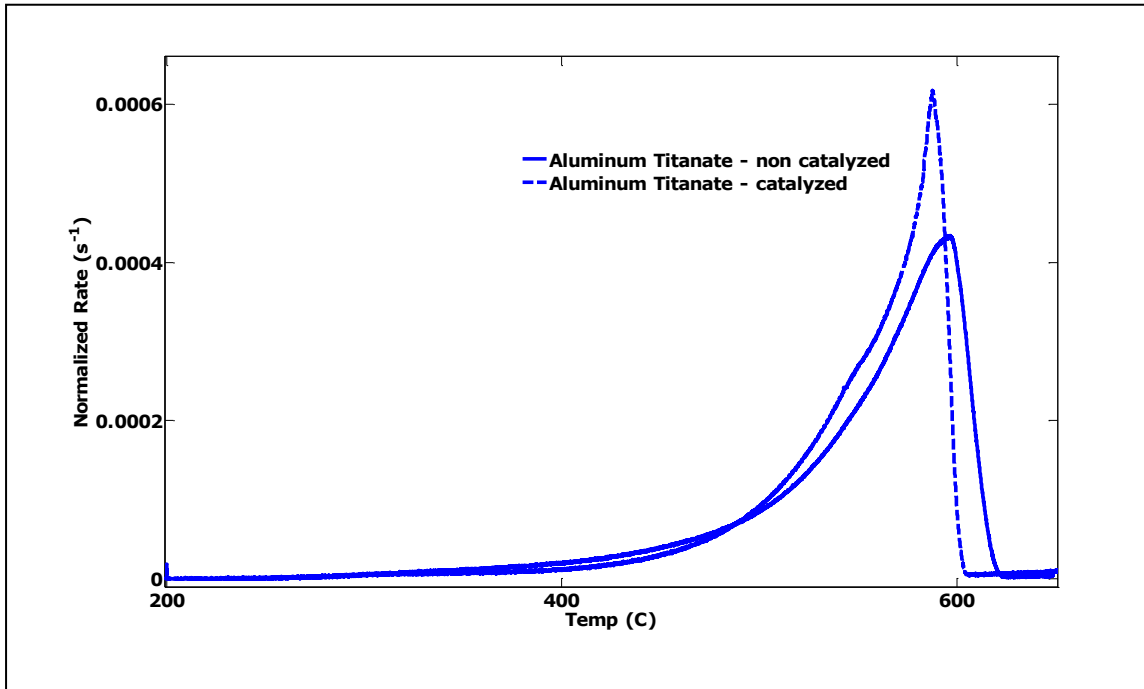
### 5.1.2 Catalyzed DPF Data Analysis

Active regeneration was performed on the catalyzed samples of the same three substrates to investigate the effect of catalyst on the oxidation kinetics. Total PGM loading and Pt/Pd ratio were the same of all three mini DPFs. A substrate-wise comparison of catalyzed and non-catalyzed oxidation rates for cordierite and aluminum titanate can

be seen in Figures 5.7 and 5.8 respectively. The rate of oxidation for the cordierite and aluminum titanate catalyzed substrates increases around the 450 - 500 °C temperature range as compared to their respective non-catalyzed ones. The peak of the rate of oxidation for the catalyzed cordierite sample shifts to a lower temperature ( $\sim 584$  °C and  $0.0006 \text{ s}^{-1}$ ) compared to that of the non-catalyzed sample which is around 593 °C. The peak of the rate of oxidation for the catalyzed aluminum titanate sample shifts to a lower temperature ( $\sim 587$  °C and  $0.0006 \text{ s}^{-1}$ ) compared to that of the non-catalyzed sample which is around 595 °C.



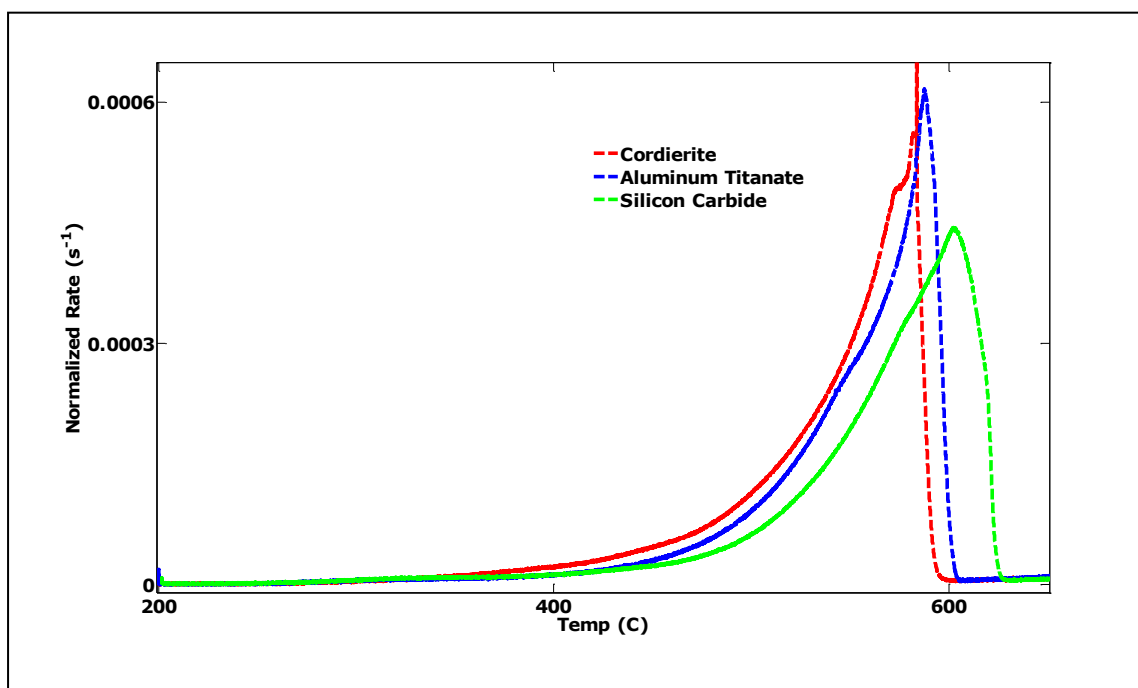
**Fig 5.7:** Rate of PM oxidation for catalyzed and non-catalyzed cordierite samples



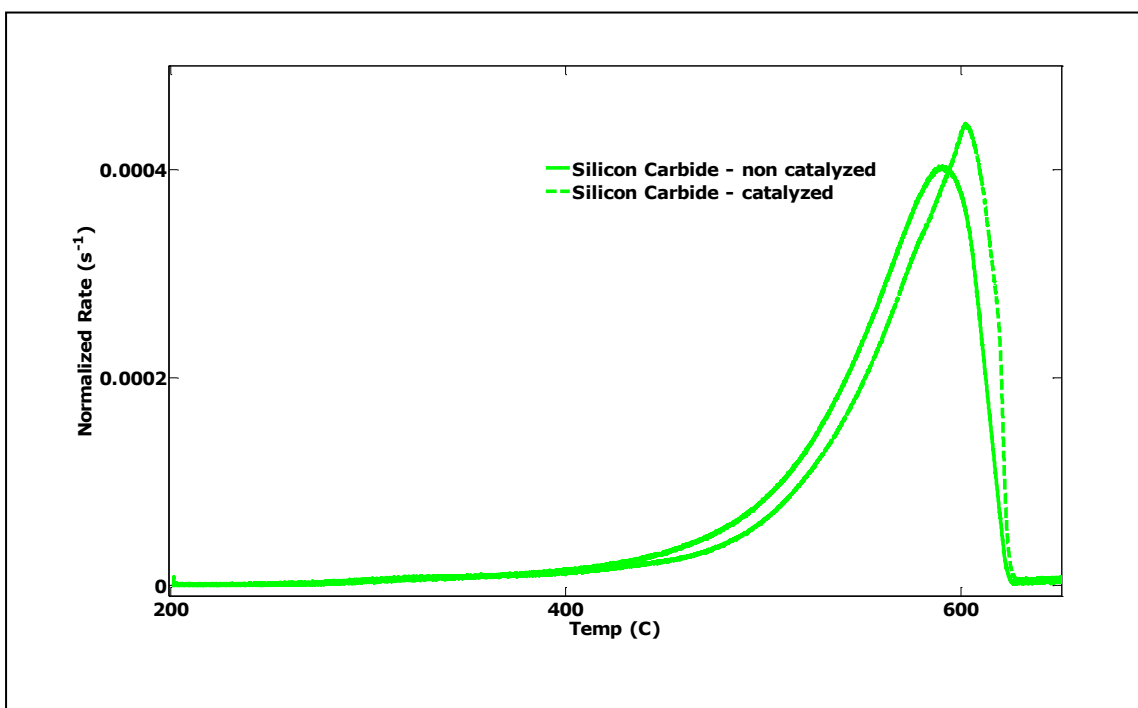
**Fig 5.8:** Rate of PM oxidation for catalyzed and non-catalyzed aluminum titanate samples

But in the case of silicon carbide, the rate of oxidation in the catalyzed sample was found to be slower than that of the non-catalyzed sample. Figure 5.10 shows this behavior of SiC where the dashed curve (catalyzed) lags behind the solid (non-catalyzed) one. The peak of the rate of oxidation for the catalyzed silicon carbide sample shifts to a higher temperature ( $\sim 603$  °C and  $0.00045$  s $^{-1}$ ) compared to that of the non-catalyzed sample which is around  $592$  °C.

The comparison of the normalized oxidation rates for the 3 catalyzed samples is shown in Figure 5.9. It can be seen that the oxidation in silicon carbide is slower than that in the cordierite and aluminum titanate substrates. This needs to be investigated further.



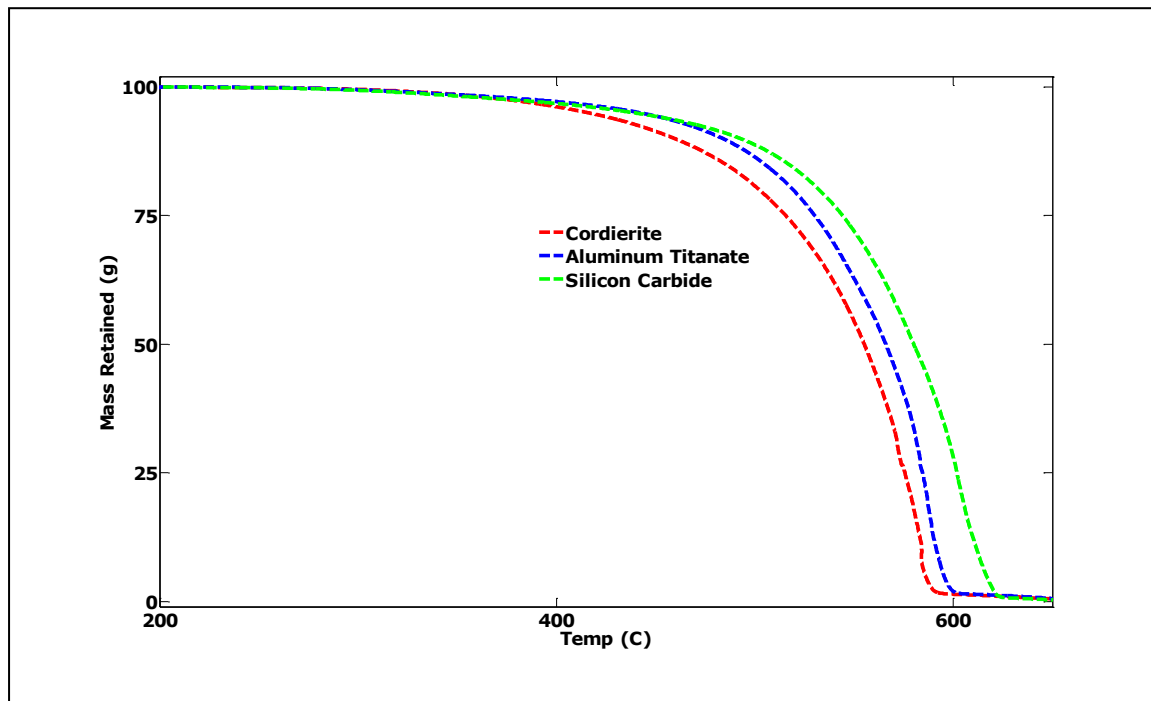
**Fig 5.9:** Rate of PM oxidation for all catalyzed samples



**Fig 5.10:** Rate of PM oxidation for catalyzed and non-catalyzed silicon carbide samples

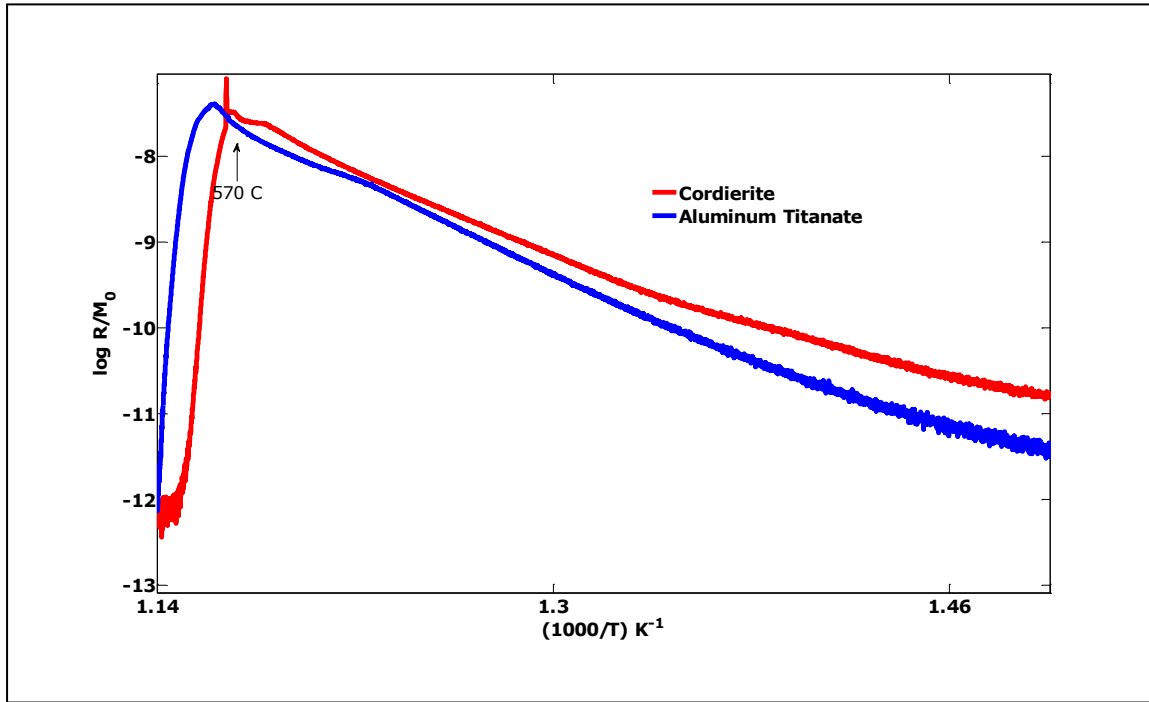
The initial mass present in the three substrates is different. The actual rates are divided by the initial mass to obtain the normalized rates. The rate of oxidation peaks at about 585 °C. The comparison of the normalized rates can be seen in Figure 5.9. The cordierite sample has the highest peak at  $0.0006 \text{ s}^{-1}$ . The aluminum titanate sample also has a peak at  $0.0006 \text{ s}^{-1}$ . The silicon carbide sample has a peak at  $0.00045 \text{ s}^{-1}$  which is 25% lesser than the cordierite sample.

Figure 5.11 shows the normalized mass profiles for the three samples. Cordierite shows maximum pre-oxidation of approximately 7 %. Aluminum titanate and silicon carbide show lower pre-oxidation of about 5 %.



**Fig 5.11:** Normalized mass retained for three different catalyzed substrates

Figure 5.12 shows the Arrhenius plot of the experimentally calculated rate. It is linear till about 575 °C. After that it curves downwards.



**Fig 5.12:** *Experimental Arrhenius Plot for two different catalyzed substrates*

Performing calculation similar to Section 5.1.1 for the catalyzed samples the value of the order of reaction  $\beta_h$  can be calculated. The Figure 5.13 shows the plot of  $\log (R/M_0)$  versus  $\log (M/M_0)$  for the high conversion regime ( $>75\%$ ). The slope or the order of reaction  $\beta_h$  is approximately 0.5, exactly similar to that for the non-catalyzed samples.

$$\log \left[ \frac{R}{M_0} \right] \text{ denotes } \ln \left[ \frac{\dot{m}_j(t)}{m_{0,j}} \right]$$

$$\log \left[ \frac{M}{M_0} \right] \text{ denotes } \ln \left[ \frac{m_j(t)}{m_{0,j}} \right]$$



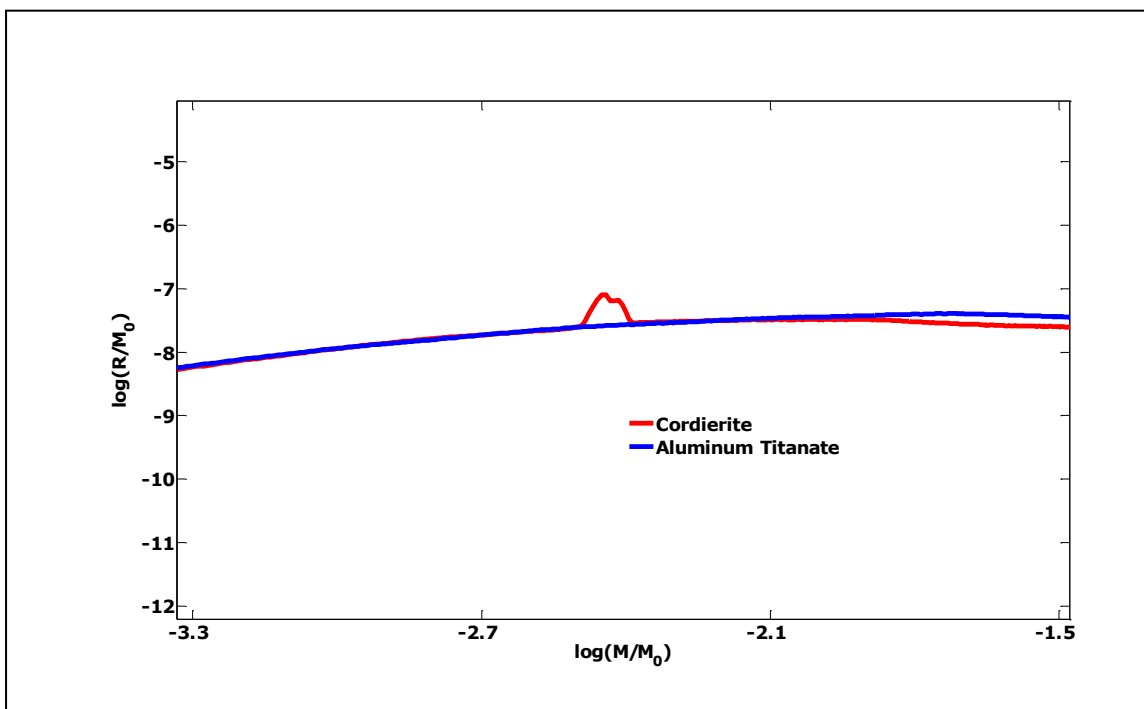


**Fig 5.13:** Calculation of  $\beta_h$  from experimental data (high conversion: ~ 75 – 100 %) – catalyzed samples

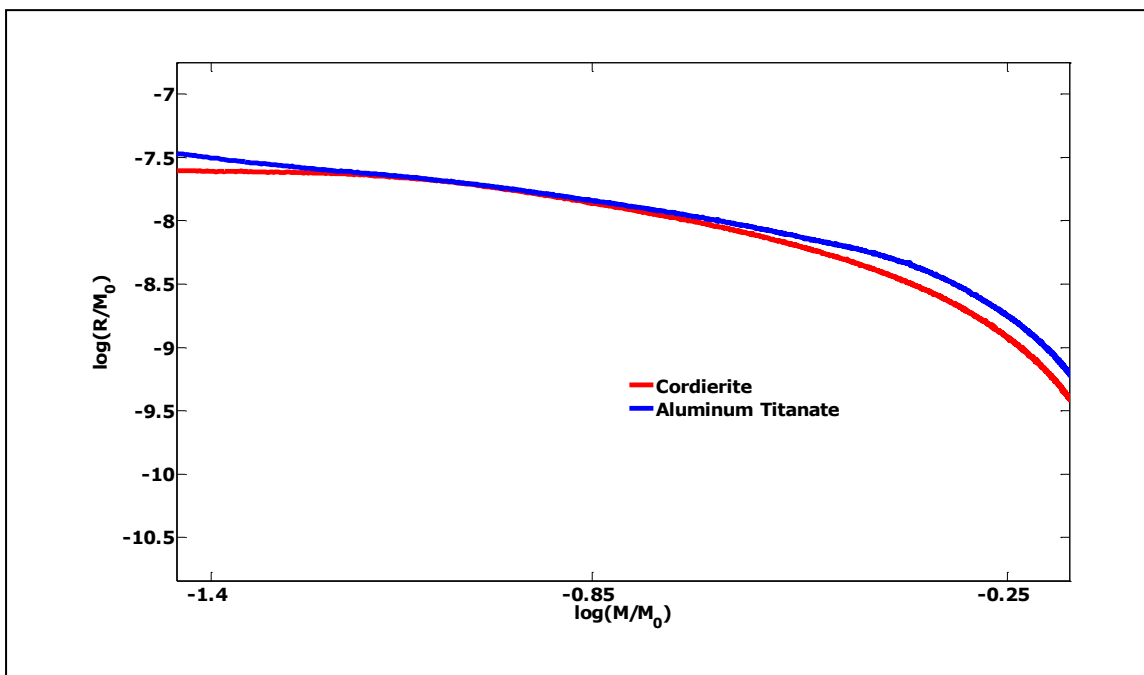


**Fig 5.14:** Calculation of  $\beta_h$  from experimental data (mid conversion: ~ 15 – 75 %) – catalyzed samples

The value of  $\beta_h$  during this mid conversion range (15 – 75 %) is roughly -1 for a major part. This suggests that the rate of oxidation is inversely proportional to the conversion. Results in (6 and 12) have reported values between 0.49 and 0.8. The Arrhenius plot in Figure 5.12 is linear in this region. Thus, it means that the order of reaction is close to 1.

The value of  $\beta_l$  for LE PM is not computed in similar fashion as the range of conversion in the pre-oxidation region (below 425 °C) is less than 10% of total mass. Thus the value of the term  $\frac{m_j(t)}{m_{0,j}}$  is very close to 1. As a result, its power does not have a significant impact.

The rate of depletion of the LE PM occurring at lower temperatures (below ~425 °C) is assumed to be of the classical Arrhenius form used in the references (11-14, 18). That is the order of reaction  $\beta_l$  is assumed to be 1. This simplifies the model.

## 5.2 Parameter Optimization Process Description

This subsection describes in detail the optimization routine that was used to estimate the kinetic parameters for the model. The *fmincon* function, a gradient based constrained optimization routine in MATLAB's optimization toolbox was used for this process.

### 5.2.1 Kinetic Parameters

Based on the model form discussed in Chapter 3, three different sets of pre-exponential factors and activation energies were estimated from equations 3.3, 3.4 and 3.5. The orders of PM retention degrees for both the HE as well as the CT PM were also determined ( $\beta_h$  and  $\beta_c$ ). The initial conditions of mass are expressed in equations 3.7, 3.8 and 3.9 (rewritten below)

$$m_{0,l} = \theta \lambda m_0 \quad \dots \dots \dots (3.7)$$

$$m_{0,h} = (1-\theta) \lambda m_0 \quad \dots \dots \dots (3.8)$$

$$m_{0,c} = (1-\lambda)m_0 \quad . . . . . \quad (3.9)$$

The values of  $\theta$  and  $\lambda$  are also estimated using the optimization routine. Thus there are a total of 10 parameters to calibrate the model. The parameters are listed in Table 5.2. Check marks are used to indicate if they are used in the optimization process.

### 5.3 Optimization Problem Setup

The parameter identification can be cast as a constrained optimization problem. The cost function  $J$  has to be minimized subject to equality and inequality constraints for all parameters and the model equations 3.4, 3.5 and 3.6.

Table 5.2 below lists the parameters that are used in the optimization for the catalyzed and non-catalyzed samples. A 'x' mark indicates that the particular parameter was not used for the particular type of samples. A '√' mark indicates that that the parameter was optimized for that particular sample. A numerical value indicates that though the parameter was used, it was not optimized.

Thus,

- |        |  |
|--------|--|
| x      | - not used                             |
| √      | - used and optimized                   |
| Number | - used but not optimized (fixed value) |

**Table 5.2**  
List of parameters

Parameter	Non Catalyzed	Catalyzed
$A_l$	✓	✓
$E_l$	✓	✓
$A_h$	✓	✓
$E_h$	✓	✓
$A_c$	x	✓
$E_c$	x	✓
$\beta_l$	1	1
$\beta_h$	✓	✓
$B_c$	x	✓
$\lambda$	1	✓
$\theta$	✓	✓

Thus the optimization problem can be written as

Minimize the cost function of Equation 5.1 subject to:

$$lb \leq \overline{x_0} \leq ub$$

where,

$$\overline{x_0} = x[A_l, E_l, A_h, E_h, \beta_h, \theta] \text{ for non-catalyzed samples and}$$

$$\overline{x_0} = x[A_l, E_l, A_h, E_h, A_c, E_c, \beta_h, \beta_c, \lambda, \theta] \text{ for non-catalyzed samples}$$

Subscripts l, h and c stand for LE, HE and CT PM. This is represented by the subscript j in equation 3.3.

### 5.3.1 Cost Function

The cost function shown in Equation 5.5 is the difference between the experimentally determined PM mass retained and the

model predicted mass retained. The optimization routine is fed with initial guesses of the kinetic parameters. The cost function calculated is then minimized by adjusting the calibration parameters. In this case, the optimization was constrained. The new set of values determined by the optimization then is used by the model and a new cost is calculated. This process continues till the minimum is found

$$J_i = \int_{t_0}^{t_f} |e_i| \, dt \quad \dots \dots \dots (5.5)$$

where  $|e_i| = |\text{Mass}_{\text{sim},i} - \text{Mass}_{\text{exp},i}|$

The cost function was computed using Euler integration as shown in Equation 5.6.

$$J_{k+1,i} = J_{k,i} + h|e_i| \quad \dots \dots \dots (5.6)$$

$J_i$  = Cost for substrate i (cordierite, aluminum titanate, silicon carbide)  
 $k$  represents time

Figure 5.15 is a schematic representation of the optimization structure wrapped around the model. The initial guesses of the kinetic parameters are the starting point of the cycle. The model predicted mass is compared to the experimentally determined mass and a cost function represented by Equations 5.5 and 5.6 is calculated. The error is minimized by the optimization algorithm used by *fmincon*. Parameter optimization was carried out individually for the three samples.

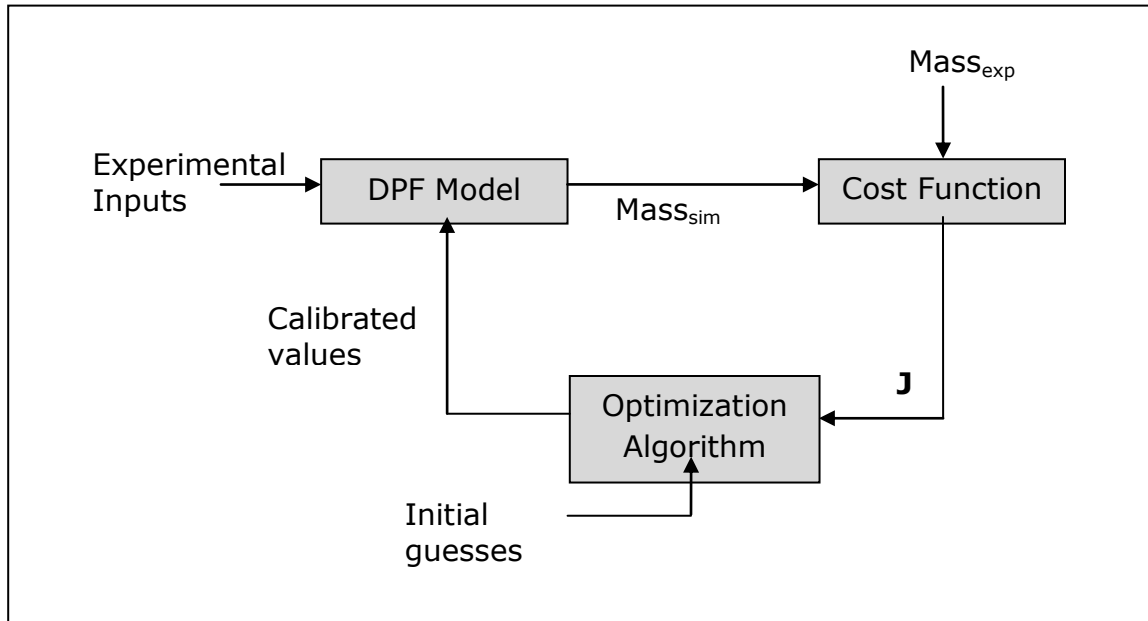


**Fig 5.15:** Schematic of optimization routine

## 5.4 Optimization Results

The *fmincon* function in MATLAB is a constrained optimization function. One of the main constraints applied during optimization was to the activation energy ( $E_h$ ) of the HE PM oxidation. This was based on the literature reported range of values as cited in reference (13). The constraints for  $\beta_h$  and  $\beta_c$  were between 0 and 1. This is based on the values in the literature (6, 12).

### 5.4.1 Results for non-catalyzed DPF samples

The model predicted mass retained for the three non-catalyzed substrates cordierite, aluminum titanate and silicon carbide are shown in Figures 5.16, 5.18 and 5.20 respectively. Figures 5.17, 5.19 and 5.21 show corresponding error bars.

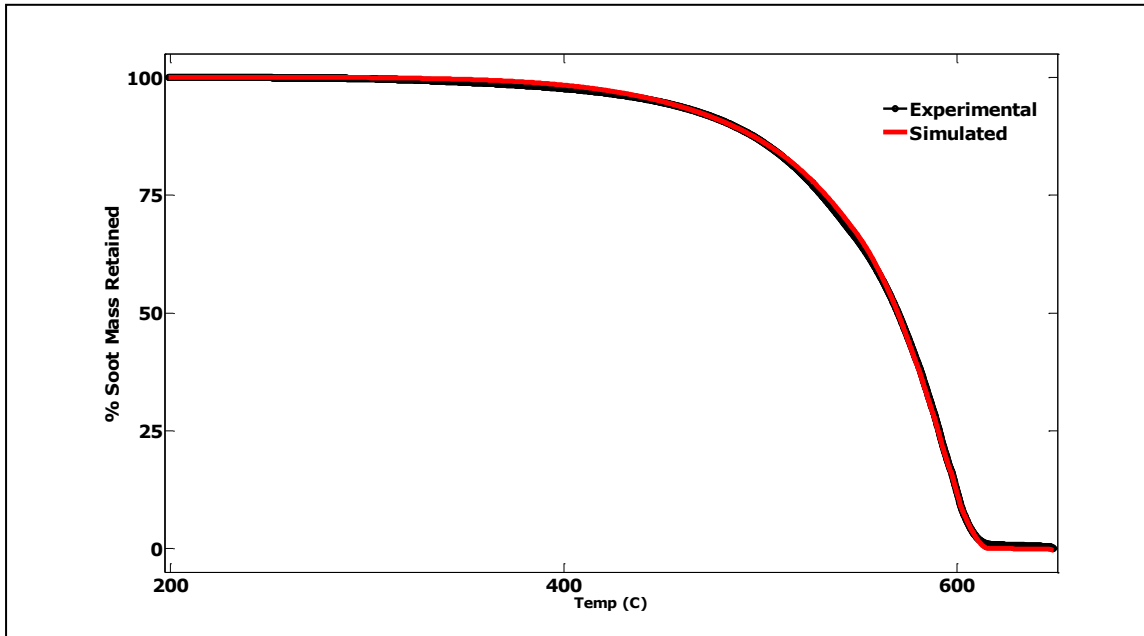


**Fig 5.16:** *Cordierite non catalyzed sample- experimental versus simulated mass retained*

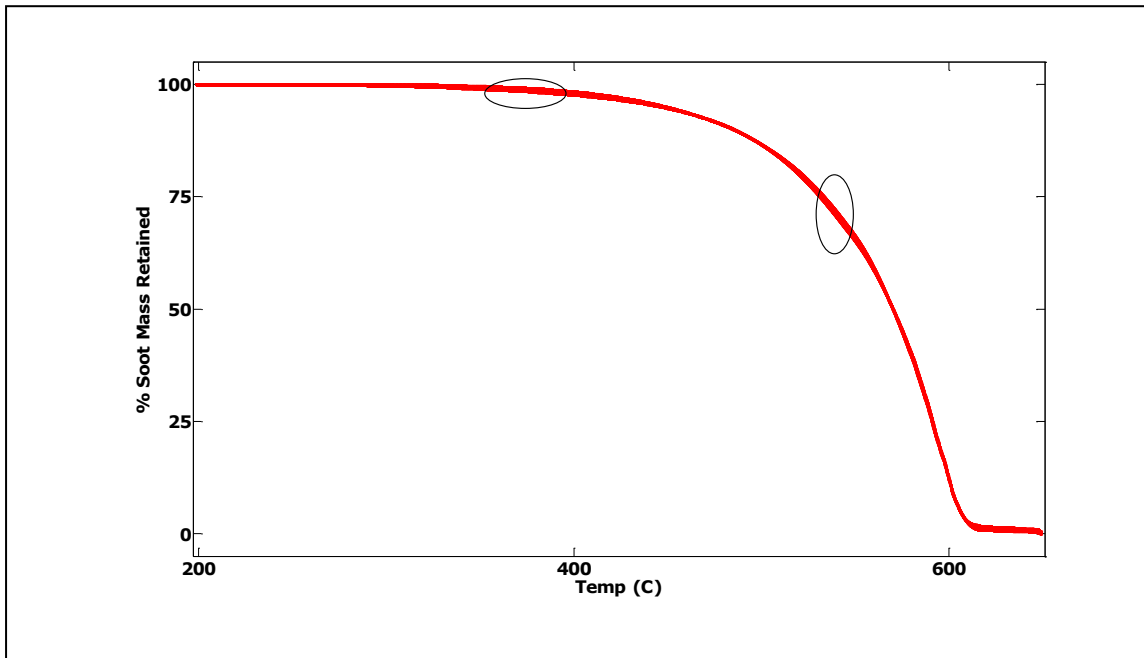


**Fig 5.17:** *Cordierite non catalyzed sample- experimental versus simulated mass retained – Error bar*

The result for the cordierite sample shows an excellent fit between the experimental and simulated data. This can be seen from

Figure 5.16. The mean squared error is very low ( $MSE = 1.38E -9$ ). The error bar plot in Figure 5.17 shows that the error regions are mostly around temperatures ranges 375 - 425 °C and 500 - 530 °C.

The result for the aluminum titanate sample also shows an excellent fit between the experimental and simulated data. This can be seen from Figure 5.18. The mean squared error is again very low ( $MSE = 1.88E -9$ ). The error bar plot in Figure 5.19 shows that the error regions are mostly around temperatures ranges 375 - 425 °C and 500 - 530 °C. Exactly similar trend is observed for the silicon carbide sample as well. This can be seen from Figures 5.20 and 5.21. The MSE for SiC is  $3.38E -9$ .

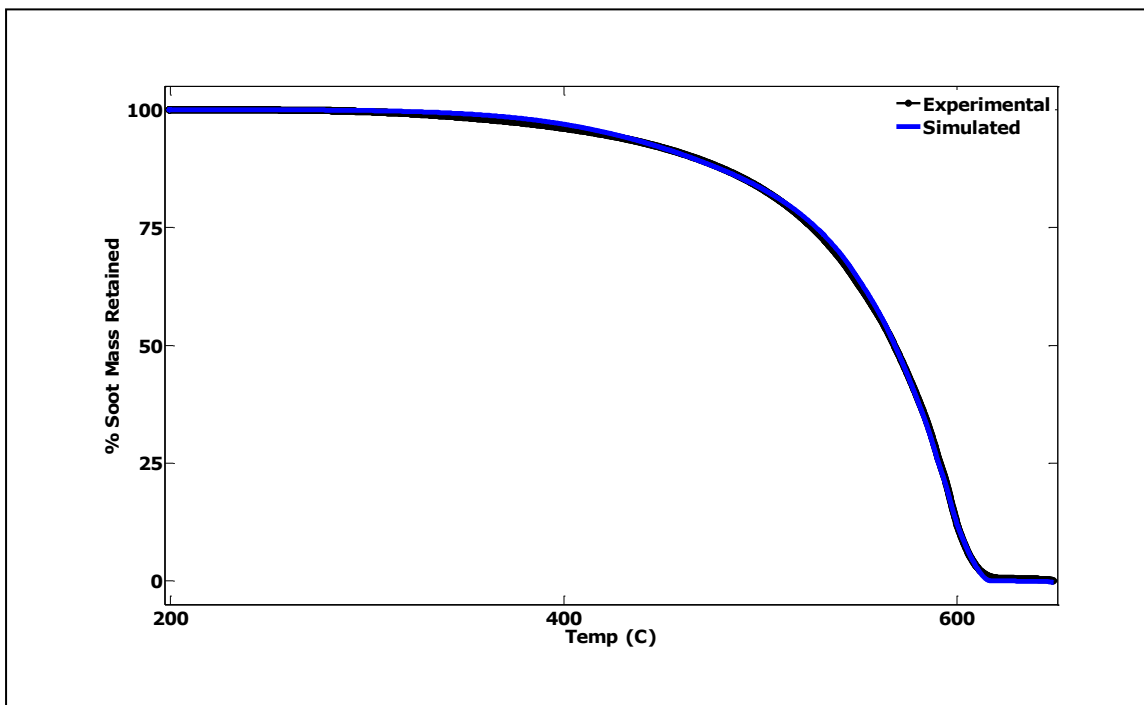


**Fig 5.18:**  $AlTi_2O_5$  non catalyzed sample- experimental versus simulated mass retained



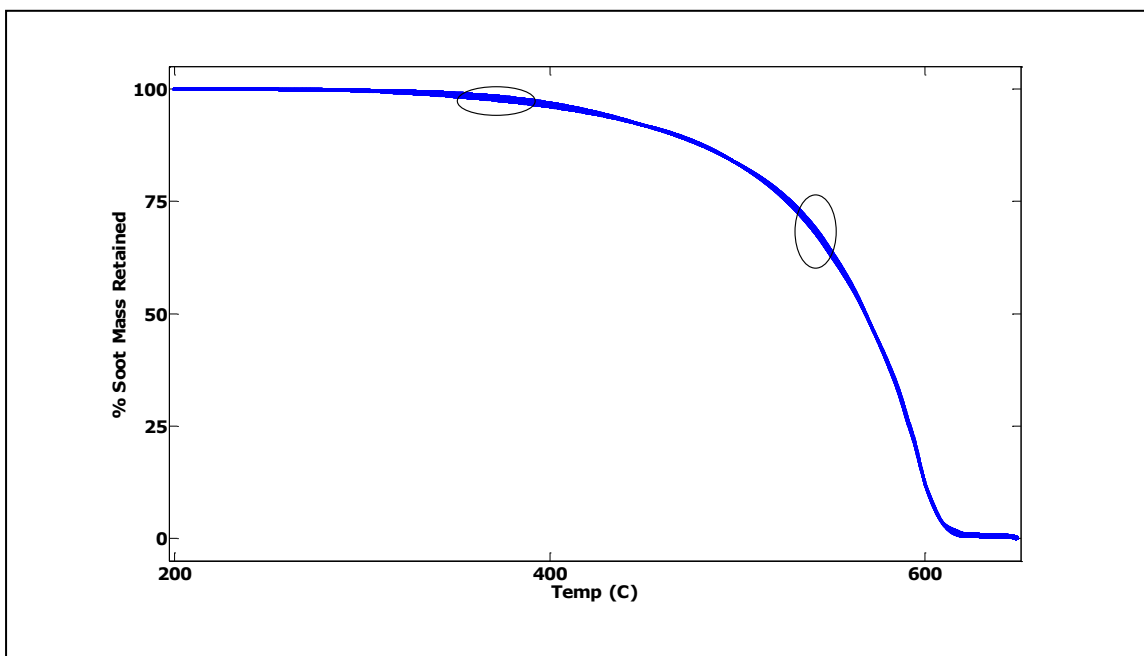


**Fig 5.19:**  $\text{AlTi}_2\text{O}_5$  non catalyzed sample- experimental versus simulated mass retained – Error bar

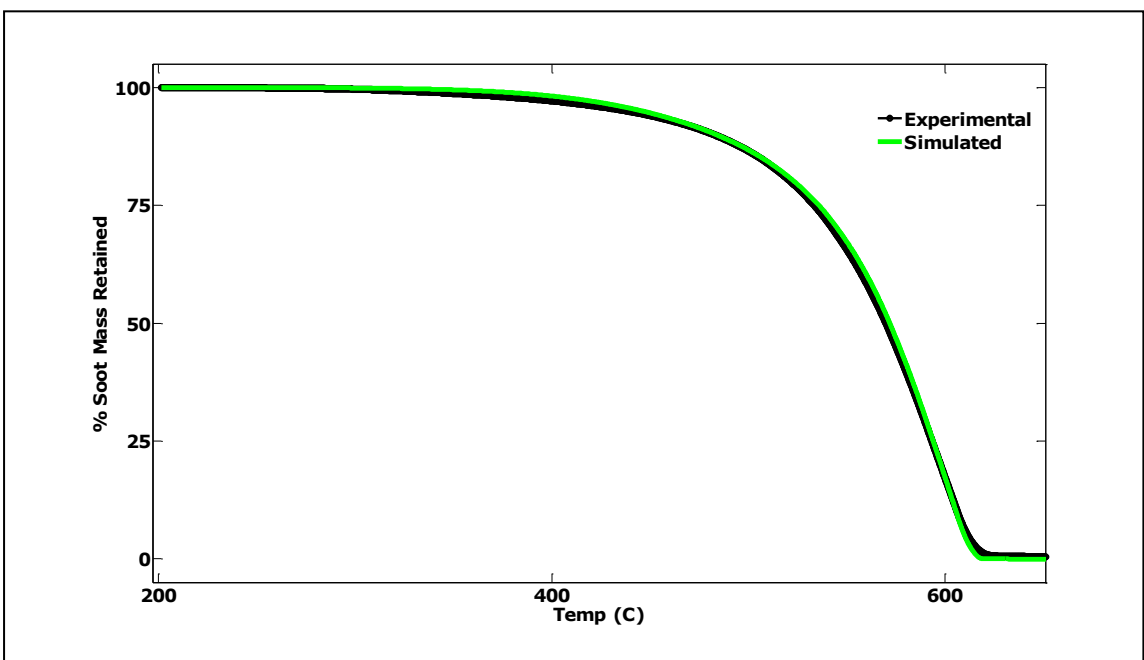


**Fig 5.20:** SiC non catalyzed sample- experimental versus simulated mass retained

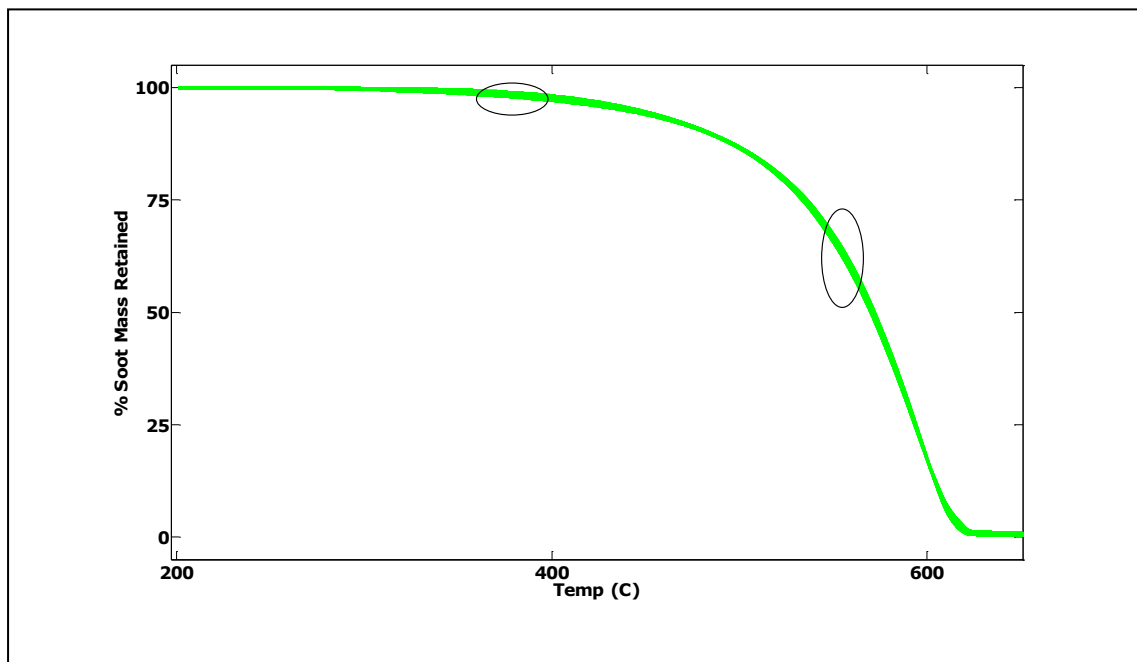


**Fig 5.21:** *SiC non catalyzed sample- experimental versus simulated mass retained- Error bar*

Optimization results are listed for all the three samples in Table 5.3.

**Table 5.3**  
Kinetic Parameters from optimization (non catalyzed)

Parameters	Cordierite	AlTi <sub>2</sub> O <sub>5</sub>	SiC	Mean Deviation %
A <sub>l</sub> (s <sup>-1</sup> )	471.50	479.00	462.00	1.2 %
E <sub>l</sub> (kJ/mol)	84.50	81.80	83.75	1.2 %
A <sub>h</sub> (s <sup>-1</sup> )	3.67E+06	3.62E+06	3.65E+06	0.5 %
E <sub>h</sub> (kJ/mol)	158.75	158.90	159.35	0.1 %
θ (n.d)	0.11	0.13	0.11	7.6 %
β <sub>h</sub> (n.d)	0.50	0.50	0.50	0

The equation for the percent mean deviation is shown in Equations 5.7 and 5.8

$$\text{Mean Deviation MD} = \frac{\sum |x - \bar{x}|}{n} \quad \dots\dots\dots (5.7)$$

$$\% \text{ Mean Deviation} = \frac{\text{MD}}{\bar{x}} \times 100 \quad \dots\dots\dots (5.8)$$

where,

$x$  = individual value of a parameter

$\bar{x}$  = mean of all the values of a parameter

$n$  = total population (3 in this case)

We can see from the mean deviation values in Table 5.3 that the values of parameters for the three substrates are very close to each other. The fraction of LE PM  $\theta$  is also within 0.11 – 0.13 for the 3 samples. The substrate material does not have any effect on the PM oxidation kinetics. The value of  $\lambda$  is set to 1 as there is no catalyst present (equations 3.7, 3.8 and 3.9). The simulation results listed in Table 5.3 shows that the optimization gives a value of 0.5 for the three samples. Thus, the value of  $\beta_h = 0.5$  works for the entire HE oxidation simulation even though the value of  $\beta_h$  obtained from Section 5.1 is not 0.5. This means that the order of reaction dominates the kinetics for the high conversion domain (over ~75 %). It also means that the order of reaction is not a contributing factor during the mid-conversion range HE oxidation (15 - 75 %). Conversion being directly proportional to surface area (5), the dependence of surface area on HE kinetics is only during high conversion regimes.

#### 5.4.1.1 Arrhenius Parameters

The pre-exponential factors and activation energy for the three substrates are very close to each other ( $159 \pm 0.2\%$ ), indicating that the oxidation behavior is independent of substrate material for non-catalyzed substrates. The values of  $E_h$  are in agreement with the values reported in literature (Table 2.1).

Figure 5.22 shows the Arrhenius plot of the simulated parameters for all the three samples.  $R$  is the rate of oxidation corresponding to model in Equation 3.1. The dashed lines show the LE

PM curve while the solid ones of the corresponding color show the HE PM curves. The rate of oxidation for LE PM is dominant in the region up to 425 °C and the HE PM oxidation dominates the regeneration in at the higher temperatures (above 480 °C). The curves lose their linear form at higher temperatures ( $\sim 590$  °C). This is the high conversion zone ( $> 75\%$ ). This shows that the order of reaction  $\beta_h$  defines the kinetics in the high conversion regimes.

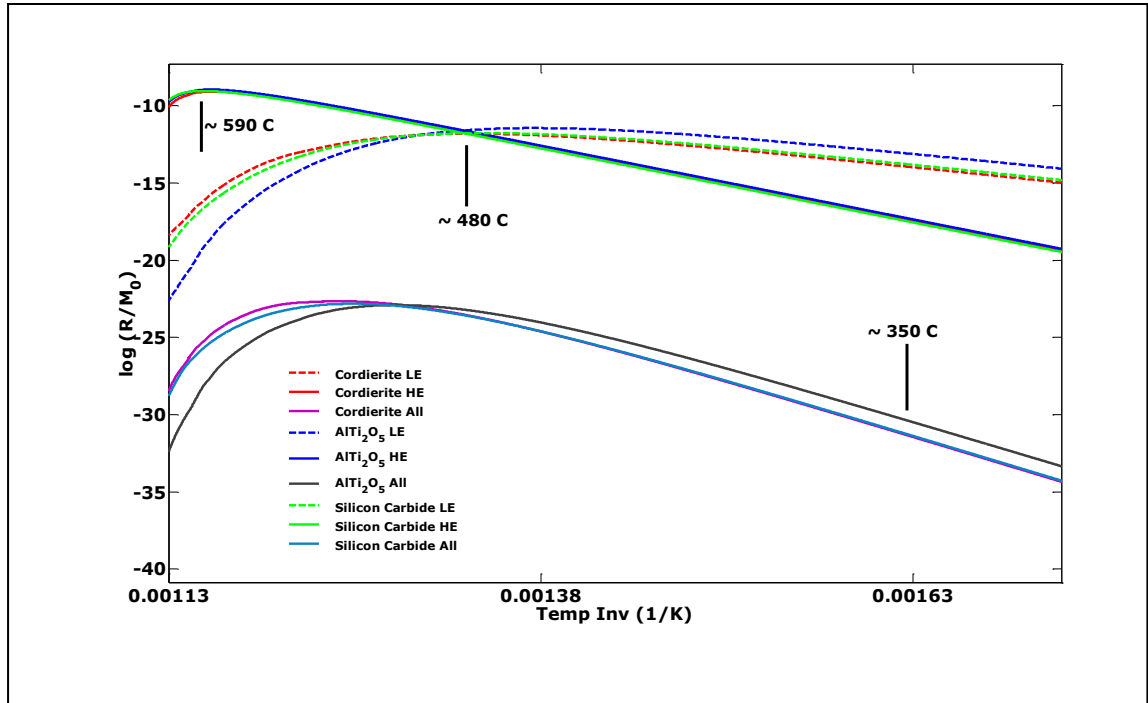


**Fig 5.22:** Arrhenius plot of simulated parameters of the three non-catalyzed samples

#### 5.4.1.2 Impact of other parameters

The order of carbon for HE PM ( $\beta_h$ ) was estimated to be 0.5 for all three samples. This value was consistently obtained from the optimization from various starting points. Thus we can say that the reaction rate is directly proportional to the square root of the instantaneous mass. The values reported in (6, 12) are in the range of 0.49 to 0.8 for conversion rates roughly in the range of 20 - 90%. The shrinking core model value mentioned in (6, 12 and 13) is roughly 0.67 and reasonably close to the value obtained from the optimization (0.5). Thus a value of 0.5 which is at the bottom of the range of values

reported in the literature shows that the PM oxidation has a high dependence on the degree of PM conversion.

The amount of PM oxidized in the pre-oxidation (LE PM) is also similar in quantity for all the samples,  $\theta = 12 \pm 1$  % of the total mass. Thus the Arrhenius form reduces to the classical form for the modeling of LE PM.

#### **5.4.2 Results for catalyzed DPF samples**

The non-catalyzed parameter values obtained were used in the simulation of catalytic oxidation. The upper and lower bounds on them were set very tight (3 % above and below). Initial guesses used for the values pertaining to catalytic oxidation were from the literature, close to values reported in reference (6).

Figures 5.23 and 5.25 show the results of the simulation compared to the experimental data for the cordierite and aluminum titanate samples respectively. The fit is reasonably close in the high conversion zones ( $\sim 90 - 100\%$  conversion). The model predicts PM mass accurately in the mid conversion regions ( $\sim 12 - 90$  %) and the pre-oxidation regions (below 12%).

We can see from the mean deviation values in Table 5.3 that the values of the parameters for the two samples are close to each other. The fraction of LE PM ( $\theta$ ) is within 0.08 – 0.12 for the two samples.

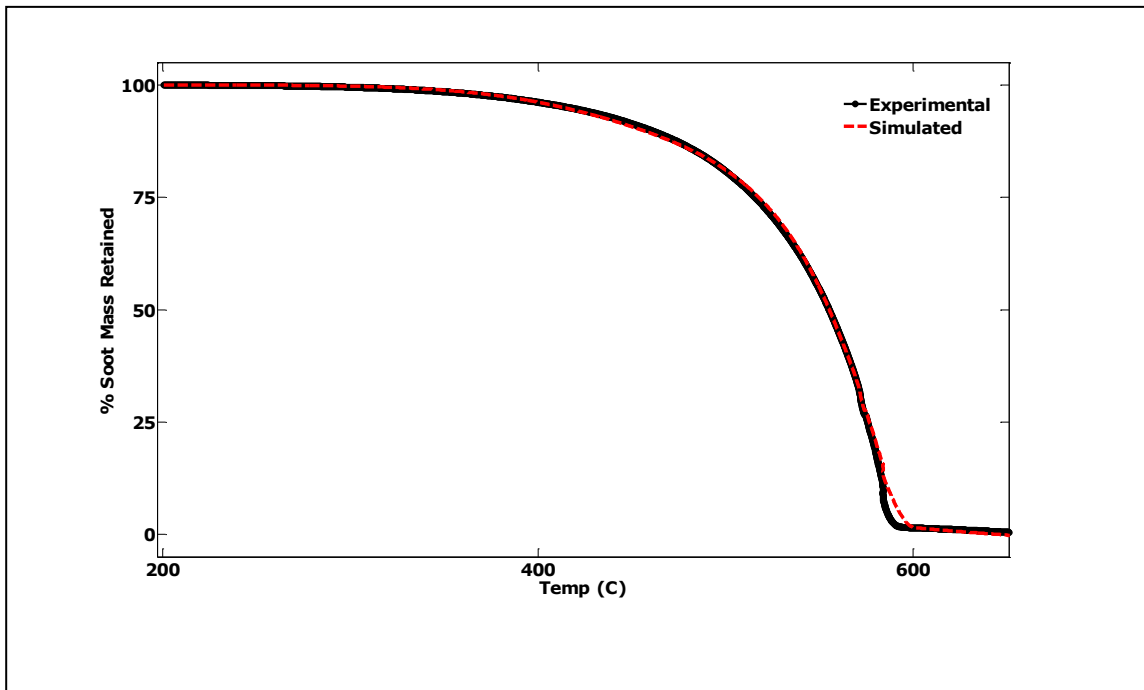


**Fig 5.23:** *Cordierite catalyzed sample- experimental v simulated mass retained*

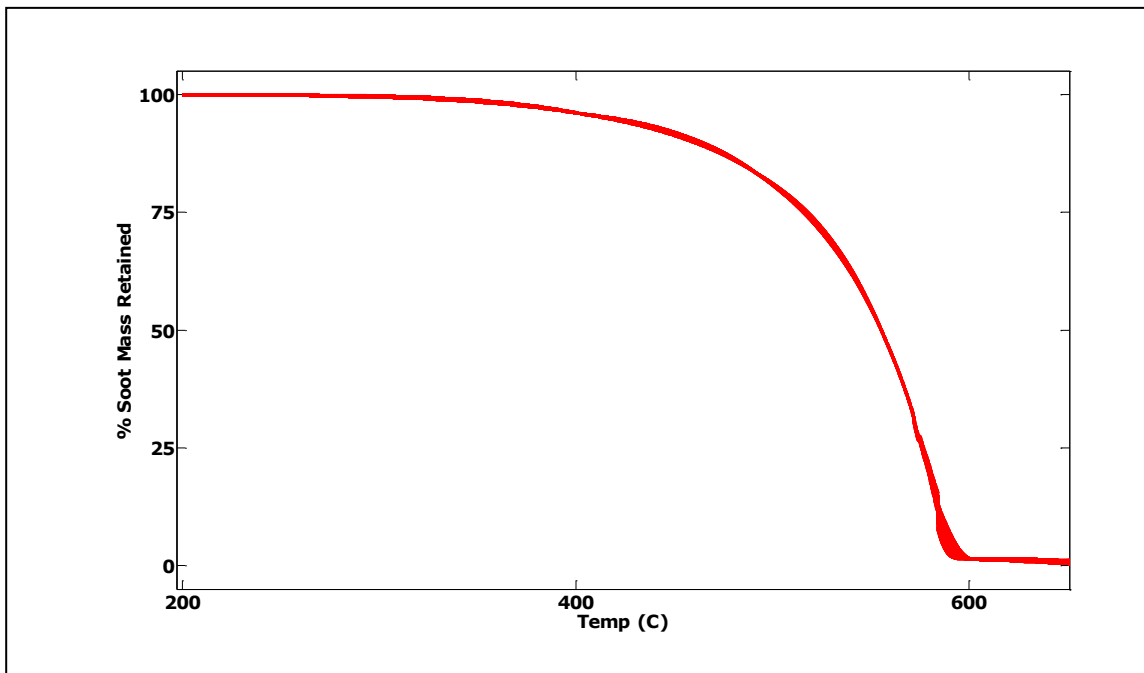


**Fig 5.24:** *Cordierite catalyzed sample- experimental v simulated mass retained –Error bar*

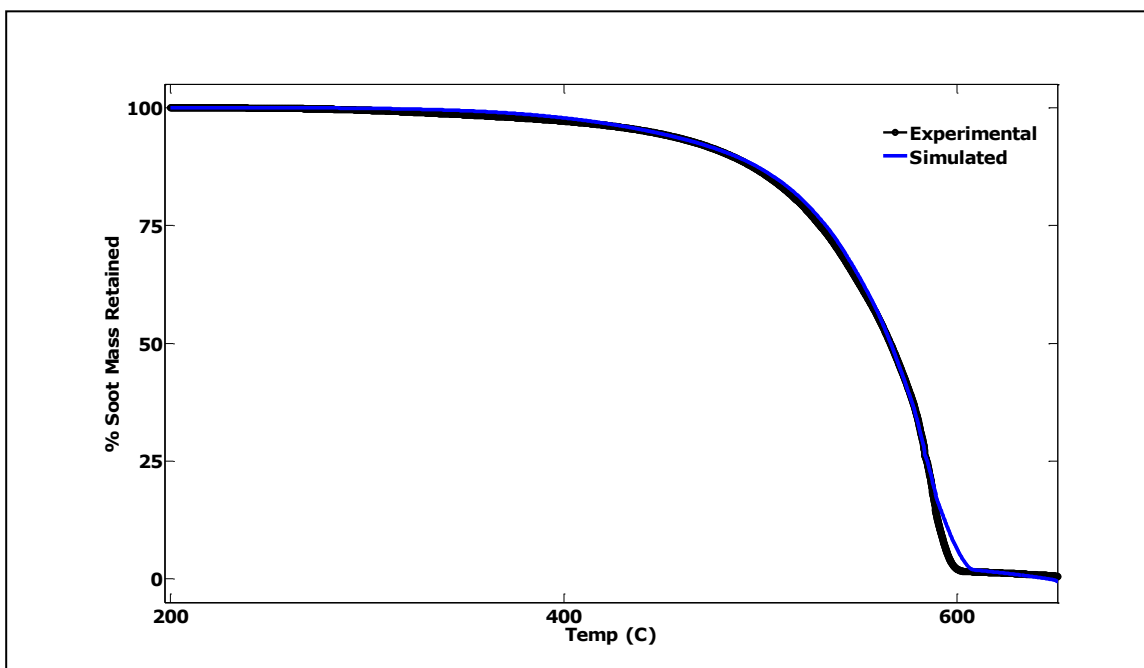


**Fig 5.25:**  $AlTi_2O_5$  catalyzed sample- experimental v simulated mass retained

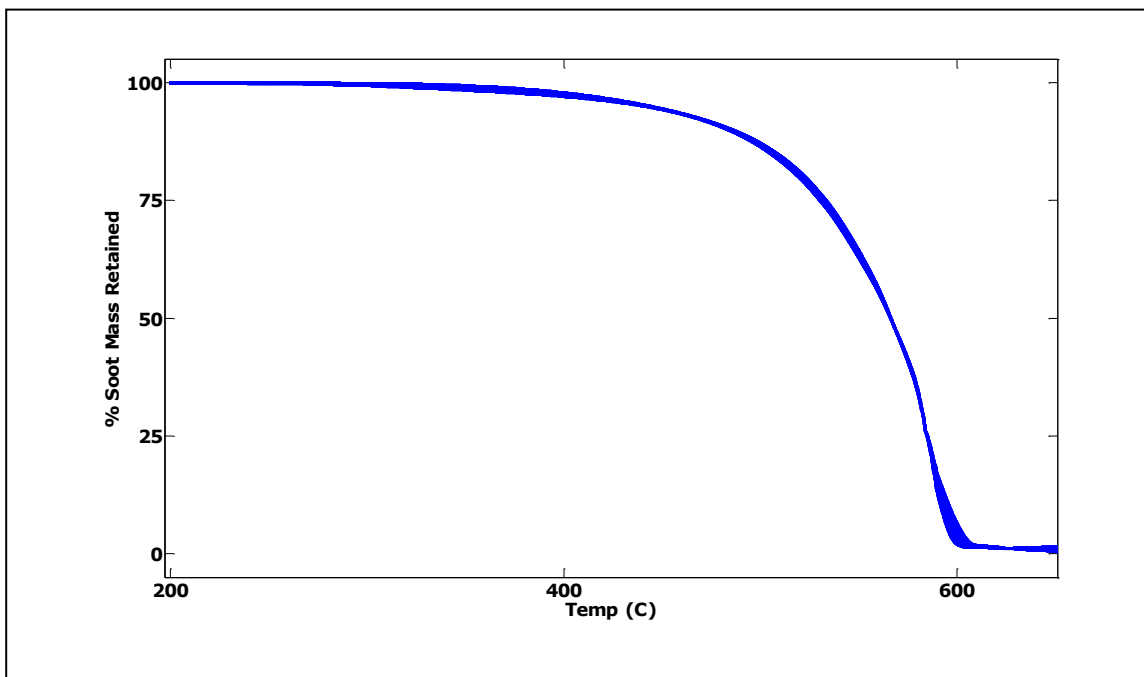


**Fig 5.26:**  $AlTi_2O_5$  catalyzed sample- experimental v simulated mass retained- Error bar

**Table 5.4**  
Kinetic Parameters from optimization (catalyzed)

Parameters	Cordierite	AlTi <sub>2</sub> O <sub>5</sub>	Mean Deviation %
A <sub>l</sub> (s <sup>-1</sup> )	446.00	435.00	1.2 %
E <sub>l</sub> (kJ/mol)	79.30	79.50	0.1 %
A <sub>h</sub> (s <sup>-1</sup> )	3.78E+06	3.54E+06	3.2 %
E <sub>h</sub> (kJ/mol)	156.15	157.20	0.3 %
A <sub>c</sub> (s <sup>-1</sup> )	8850.00	8842.00	0.05 %
E <sub>c</sub> (kJ/mol)	117.65	120.20	1.1 %
λ (n.d)	0.95	0.95	0
θ (n.d)	0.12	0.08	20 %
β <sub>h</sub> (n.d)	0.50	0.49	1 %
β <sub>c</sub> (n.d)	1.0	1.0	0

#### 5.4.2.1 Arrhenius Parameters

The pre-exponential factors and activation energy for the 2 substrates are fairly close to each other as indicated by the mean deviation values in Table 5.4. This indicates that the oxidation behavior of HE PM is not affected by the catalyst. It seems that once the CT PM has burned out the remaining oxidation corresponds to the HE PM oxidation. Values of E<sub>c</sub> are in agreement with the values reported in literature (6). The rates of catalytic oxidation for the 2 substrates are almost equal as the mean deviation values of the activation energy (E<sub>c</sub>) and pre-exponential (A<sub>c</sub>) are within 1 %.

Figure 5.27 shows the Arrhenius plot of the simulated parameters for all the samples. R is the rate of oxidation corresponding to model in Equation 3.1. The bolder dashed lines show the LE PM curve while the solid ones of the corresponding color show the HE PM curves. The comparatively lighter dashed lines show catalytic oxidation curve. The rate of oxidation for LE PM is dominant



in the region up to 425 °C and the HE PM oxidation dominates the regeneration in at the higher temperatures (above 480 °C).

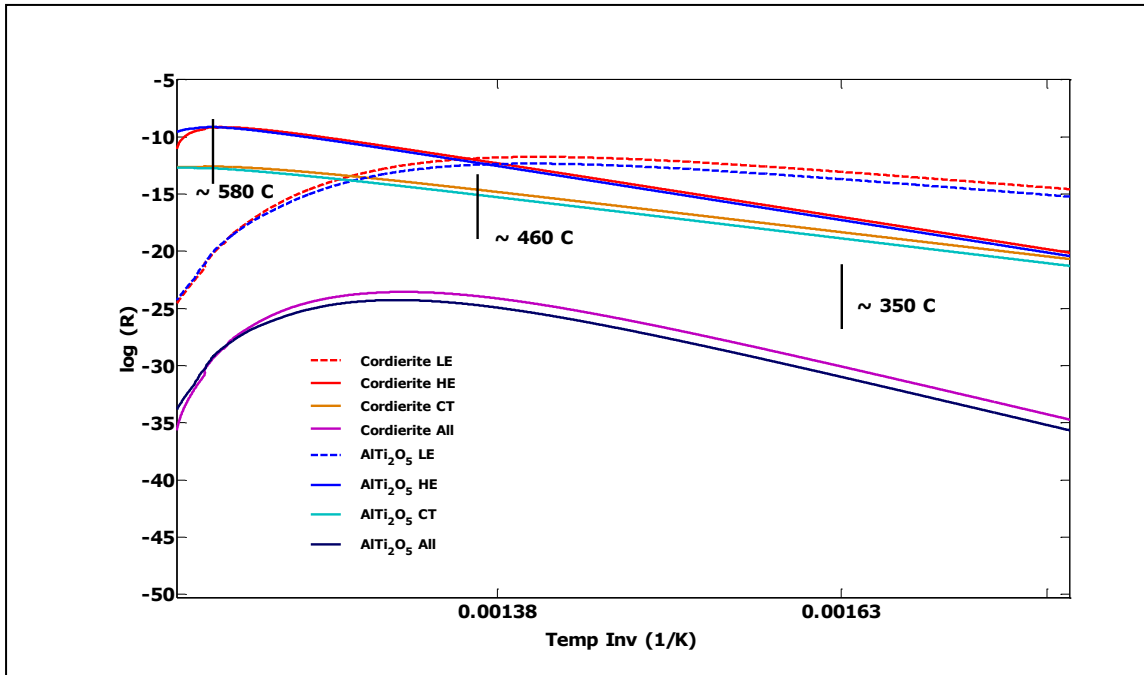


**Fig 5.27:** Arrhenius plot of simulated parameters of the three catalyzed samples

The catalytic oxidation does not seem to be dominant in any particular temperature or conversion regime. The curve loses its linear form at higher temperatures ( $\sim 575$  °C). This is the high conversion zone ( $> 70$  %). This shows that the order of reaction  $\beta_h$  defines the kinetics in the high conversion regimes.

#### 5.4.2.2 Impact of other parameters

The values of  $\beta_h$  for both samples were estimated to be 0.5 as was the case for non-catalyzed samples. This shows that the order of conversion for HE PM is not affected by the application of catalyst washcoat. High values of  $\lambda$  show that the amount of PM not in contact with the catalyst (HE PM) is very high due to the 7 g/l loading. The values of  $\beta_c$  for both samples were estimated to be 1. This means that the catalyzed oxidation is not surface area dependent.

The Tables 5.5 and 5.6 give a substrate by substrate comparison of the kinetic parameters. In the case of cordierite (Table 5.5) and

aluminum titanate (Table 5.6) we can clearly see from the mean deviation values (which are within a maximum of 5 %) that the catalyst has no significant effect on the HE PM oxidation kinetics. Once the LE PM is burned out, the catalytic oxidation starts. Once the CT PM is burned out, only the HE PM remains. The parameters of HE PM are independent of the either the catalyst or the substrate. Similar trend was observed in (6) and (17).

The values of mean deviation for the LE PM oxidation ( $A_l$ ,  $E_l$ ) show that there is no significant difference in the LE PM oxidation behavior due to the presence of catalyst. This is seen Tables 5.5 and 5.6. The amount of LE PM ( $\theta$ ) in catalyzed cordierite substrate is almost equal that in the non-catalyzed sample (Tables 5.5).

**Table 5.5**  
Kinetic Parameters from optimization (Cordierite)

Parameters	Cordierite		Mean Deviation %
	Non-catalyzed	Catalyzed	
$A_l$ ( $s^{-1}$ )	471.50	446.00	2.8 %
$E_l$ (kJ/mol)	84.50	79.30	3.2 %
$A_h$ ( $s^{-1}$ )	3.67E+06	3.78E+06	1.4 %
$E_h$ (kJ/mol)	158.75	156.15	0.8 %
$A_c$ ( $s^{-1}$ )	-	8850.00	-
$E_c$ (kJ/mol)	-	117.65	-
$\lambda$ (n.d)	1	0.95	-
$\theta$ (n.d)	0.11	0.12	4.3 %
$\beta_h$ (n.d)	0.50	0.50	0 %
$\beta_c$ (n.d)	-	1.0	-

But as seen in Table 5.6 we can see that the amount of LE PM is different for the catalyzed and non-catalyzed substrate. Pre-oxidation was found to occur up to a maximum of 25% of PM conversion for the Temperature Programmed Oxidation (TPO) runs in the work done in [7]. Thus this seems to be a fluctuating quantity from experiment to experiment. It is in the range of 8 - 13 % of the total mass for the data investigated in this research.

**Table 5.6**  
Kinetic Parameters from optimization (Aluminum Titanate)

Parameters	AlTi <sub>2</sub> O <sub>5</sub>		Mean Deviation %
	Non-catalyzed	Catalyzed	
$A_l$ (s <sup>-1</sup> )	479.00	435.00	4.8 %
$E_l$ (kJ/mol)	81.80	79.50	1.5 %
$A_h$ (s <sup>-1</sup> )	3.62E+06	3.54E+06	1.1 %
$E_h$ (kJ/mol)	158.90	157.20	0.5 %
$A_c$ (s <sup>-1</sup> )	-	8842.00	
$E_c$ (kJ/mol)	-	120.20	-
$\lambda$ (n.d)	1.00	0.95	-
$\theta$ (n.d)	0.13	0.08	24 %
$\beta_h$ (n.d)	0.50	0.49	1 %
$B_c$ (n.d)	-	1.0	-

## 6. **CONCLUSION AND FUTURE WORK**

A simple mathematical model for the prediction of PM mass on a DPF filter during active regeneration was developed in MATLAB/Simulink®. It was calibrated using experimental data from a Navistar 13L diesel engine and its kinetic parameters were estimated by numerical optimization techniques.

The model was developed based on the hypothesis and equations mentioned in chapter 3. For a non-catalyzed sample, there are 2 types of PM (LE and HT PM). LE PM is oxidized during the pre-oxidation described in Section 2.3. After the LE PM is oxidized, the HE PM is oxidized. In a catalyzed sample, there are 3 types of PM (LE, HE and CT). LE PM and HE PM are the same as that of the non-catalyzed sample. The CT PM is in contact with the catalyst and takes part in catalytic oxidation only. Figures 5.16, 5.18 and 5.20 shows that the simulated mass burnout profiles for non-catalyzed samples matched the experimentally deduced ones. One of the major conclusions from the study of non-catalyzed samples was the independence of PM oxidation kinetics with respect to the substrate material.

From the parameter optimization exercise, it was found that the kinetics of the HE and LE PM oxidation are not affected by the presence of catalyst washcoat. Hence this suggests that the presence of catalyst could be the reason for increase in the total PM oxidation rate.

The order of PM retention degree of CT oxidation was estimated by the optimization routine as 1. This data indicates that the catalytic oxidation is not a function of the active surface area unlike the non-catalytic PM oxidation which is dependent on the active surface area. The order of PM retention degree of HE PM ( $\beta_h$ ) assumes importance with increase in PM conversion. For very high conversion range (above 75 %) the order of reaction  $\beta_h$  is the dominating factor.

Another conclusion derived from the modeling results is that the amount of LE PM seems to vary from experiment to experiment. Though it is almost equal for the catalyzed and non-catalyzed cordierite samples, it varies by about 5 % for the catalyzed and non-catalyzed aluminum titanate samples. This can be seen in Tables 5.5 and 5.6.

Figures 5.23 and 5.25 show the fit of the oxidation profiles for the catalyzed samples. The effect of catalyst on the PM oxidation kinetics was studied. Parameters for the catalytic oxidation were

estimated. The SiC data was not modeled as it shows surprising behavior (Fig 5.10) which needs to be investigated further.

The kinetic parameters listed in Tables 5.3 and 5.4 were estimated using numerical optimization techniques.

From the knowledge gained from this research, the following future work is recommended.

1. This model predicts active regeneration behavior for a PM loading of 7 g/l and space velocity of  $40000 \text{ hr}^{-1}$ . Tests performed at different space velocities could provide a slight change in the parameters. The current model is based only on temperature programmed oxidation tests. A more detailed study of the kinetics can be performed by pulsed oxidation tests. This would mean investigating the effect of space velocity, temperature, water etc. on PM oxidation kinetics.
2. The behavior of catalyzed silicon carbide observed in Figure 5.5 is quite surprising since the rate of oxidation of the catalyzed sample is slower than that of the non-catalyzed sample (As opposed to Cordierite and Aluminum Titanate). Testing under exactly same conditions should be performed for determining if such trends are indeed repeatable or the current data is anomalous.
3. The capability of the model is limited to active regeneration only based on current needs. A passive oxidation routine can be added to this to ensure a more complete regeneration package.
4. The model can be used to develop an input temperature profile to attain a desired PM mass oxidation profile.
5. The DPFs used in the experimental work were mini DPFs (1 inch O.D X 3 inches in length). Hence the model needs to be validated under exactly similar conditions using a full sized DPF.

## **REFERENCES**

- [1] Premchand, Kiran. *An Experimental and Modeling Study of the Filtration and Oxidation Characteristics of a Diesel Oxidation Catalyst and a Catalyzed Particulate Filter*. MS Thesis, Michigan Technological University, 2006.
- [2] Hasan, Mohammed. *The Filtration and Oxidation Characteristics of a Diesel Oxidation Catalyst and a Catalyzed Particulate Filter: Development of a 1-D 2-Layer Model*. MS Thesis, Michigan Technological University, 2005.
- [3] Surenahalli, Harsha S. *A Modeling Study of a Diesel Oxidation Catalyst and Catalyzed Particulate Filter during Loading and Active Regeneration*. MS Thesis, Michigan Technological University, 2010.
- [4] Triana, Antonio Padilla. *Development of Models to Study the Emissions, Flow, and Kinetic Characteristics from Diesel Oxidation Catalysts and Particulate Filters*. PhD Thesis, Michigan Technological University, 2005.
- [5] Neeft, John P. A., Michiel Makkee, and Jacob A Moulijn. *Catalytic Oxidation of Carbon Black – I. Activity of catalysts and classification of oxidation profiles*. Fuel Vol. 77, No. 3 (Fuel Vol 77), 1998: 111-119.
- [6] Darcy, Pierre, Patrick Da Costa, Henry Mellottee, Jean-Michael Trichard, and Gerald Djega-Mariadassou. *Kinetics of catalyzed and non-catalyzed oxidation of soot from a diesel engine*. Catalysis Today 119, 2007: 252-256.
- [7] Yezerets, Aleksey, Neal W Currier, Heather A Eadler, Arvind Suresh, Paula F Madden, and Mark A Branigin. *Investigation of the oxidation behavior of diesel particulate matter*. Catalysis Today 88, 2003: 17-25.
- [8] Konstandapoulus, A G, and M Kostoglou. *Periodically Reversed Flow Regeneration of Diesel Particulate Traps*. SAE: 1999-01-0469, 1999.

- [9] Bissett, Edward. *Mathematical Model of the Thermal Regeneration of a Wall-Flow Monolith Diesel Particulate Filter*. Chemical Engineering Science 9, 1983: 1232-1244.
- [10] Premchand, Kiran C, John H Johnson, and Song-Lin Yang. *Development of a 1-D CPF Model to Simulate Active Regeneration of a Diesel Particulate Filter*. 2009 SAE World Congress, 2009: Paper No. 2009-01-1283.
- [11] Achour, Louiza, Jean-Baptiste Dementhon, and Pierre Rouchon. *Original Modeling Approach of Diesel Particulate Filter Regeneration*. SAE, 2001: SAE Paper No. 2001-01-1943.
- [12] Neeft, John P.A, Xander T Nijhuis, Erik Smakman, Michiel Makkee, and Jacob A Moulijn. *Kinetics of the oxidation of diesel soot*. Fuel Vol. 76, No. 12, 1997: 1129-1136.
- [13] Stanmore, B R, J F Brilhac, and P Gilot. *The oxidation of soot: a review of experiments, mechanisms and models*. Carbon 39, 2001: 2247-2268.
- [14] Avra, Brahma. *Modeling and Observability Analysis of DPF Regeneration*. ASME Dynamic Systems and Controls Conference, DSCC2008-2106, 2008.
- [15] Dieselnet Online Resource.  
[http://www.dieselnet.com/tech/dpf\\_regen.html](http://www.dieselnet.com/tech/dpf_regen.html) (accessed April 2011). www.DieselNet.com, Vers. Revision 2005.6a. Ecopoint Inc. 2005..
- [16] Prasad, R, and Venkateswara Rao Bella. *Isothermal Kinetics of Catalyzed Air Oxidation of Diesel Soot*. (Bulletin of Chemical Reaction Engineering & Catalysis) 5 (2), 95 - 101 (2010).
- [17] Lopez-Fonseca, R, U Elizundia, I Landa, and M A Gu. *Kinetic analysis of non-catalytic and Mn-catalysed combustion of diesel soot surrogates*. (Applied Catalysis) B, no. Environmental 61 150–158 (2005).
- [18] York, Andrew P.E, Ahmadinejad, Mehrdad and Watling, Timothy C. *Modeling of the Catalyzed Continuously Regenerating Diesel Particulate Filter (CCR-DPF) System: Model Development and Passive Regeneration Studies*. (SAE Technical Paper Series), no. 2007-01-0043.

## **APPENDIX A**

Below is the setup of the optimization/simulation code. Here, the user can set whether the model parameter values and whether they should be optimized. The 'fmincon' routine in MATLAB optimizes the model kinetic parameters. This can be bypassed by setting the runs.optimize 0.

```
% -----
% Setup data, constants and globals
% -----

clear all;
clc;
format short g
GnC;                                % Load Globals and Constants
LoadO2TPOData;                      % Experimental Data Loading

% -----
% User Inputs
% -----

runs.optimize = 0;                  % Optimize YES = 1 ; NO = 0
runs.sample = ALT;                  % Sample to simulate (COR, ALT, SIC)
runs.plotter = massvtemp;           % massvtemp, ratevtemp, massvtime,
runs.plotype = ERR;                 % NOR = normal plot, ERR = Error bar

% -----
% Experimental Data Processing
% -----

gpsconv;                            % Convert the rate to g/s
MassFromData;                       % Calculate experimental PM load in g

% -----
% Input model kinetic parameters for simulation/optimization
% -----

runs.params(A_1) = 435.00;          % A for LE soot
runs.params(E_1) = 79.50;           % E for LE soot
runs.params(A_2) = 3.54e6;          % A for HE soot
runs.params(E_2) = 157.25;          % E for HE soot
runs.params(A_3) = 8842.0;          % A for CT soot
runs.params(E_3) = 120.20;          % E for CT soot
runs.params(b_1) = 1.0;             %  $\beta$  for LE soot
```



```

runs.params(b_2) = 0.49;           %  $\beta$  for HE soot
runs.params(b_3) = 1.0;           %  $\beta$  for CT soot
runs.params(lam) = 0.95;          %  $\lambda$ 
runs.params(tht) = 0.07;          %  $\theta$ 

% -----
%           Input Upper and Lower bounds of the optimization constraints
%           A1  E1  A2  E2  A3  E3  b1  b2  b3  sdf th
% -----

runs.lb = [0.99 ; 0.99 ; 0.99 ; 0.99; 0.95; 0.98; 0.999; 0.99; 0.11; 0.98; 0.6];
runs.ub = [1.01 ; 1.01 ; 1.01 ; 1.01; 1.05; 1.02; 1.001; 1.01; 1.01; 1.02; 1.4];

runs.opts = optimset('MaxFunEvals',3000);           % # of Function Evaluations
x0 = ones(1,length(runs.params));                  % Memory Pre-allocation

% -----

if runs.optimize == 1
    xopt = fmincon(@Simulator1,x0,[],[],[],[],runs.lb,runs.ub,[],runs.opts);
else
    [ff] = Simulator1(x0);                          % No optimization takes place for this
end

```

The following flowchart further explains the code

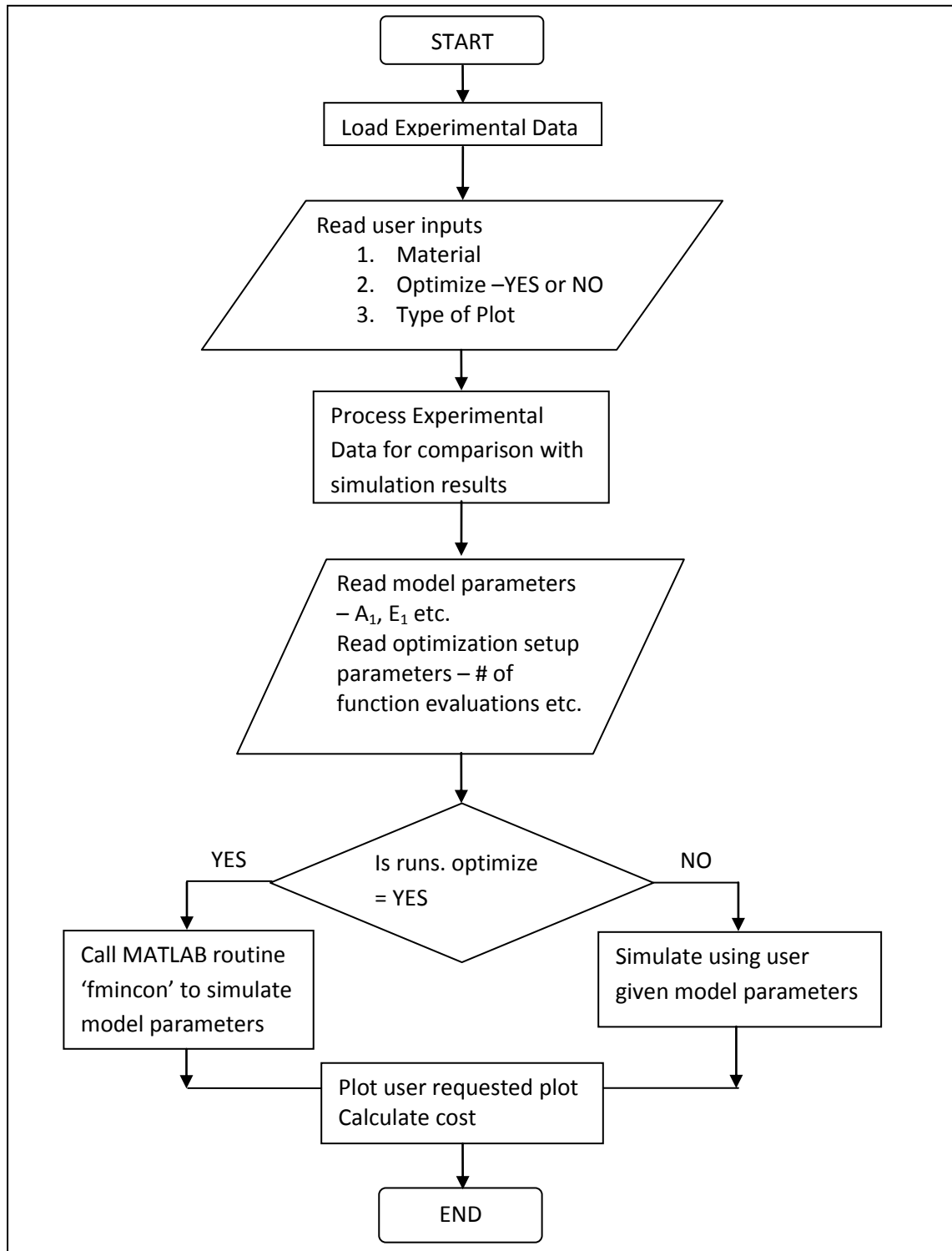


**Fig A.1:** Flowchart of the code